International Journal of Numerical Methods for Heat & Fluid Flow

ISSN: 0961-5539; Impact Factor: 2.450; **Publisher**: Emerald Publishing.

(Accepted April 11th 2019)

Magneto-Bioconvection Flow of a Casson Thin Film with Nanoparticles over an Unsteady Stretching Sheet: HAM and GDQ Computation

B. VASU[1], ATUL KUMAR RAY[1], O. ANWAR BÉG[2],RAMA SUBBA REDDY GORLA[3] †

1. Department of Mathematics, Motilal Nehru National Institute of Technology, Allahabad-211004, **India**
2. Department of Mechanical and Aeronautical Engineering, Salford University, Salford, M54WT, **UK**
3. Department of Mechanical Engineering, Cleveland State University, Ohio, 44115, **USA**

Abstract

Purpose – To numerically investigate the two-dimensional unsteady laminar magnetohydrodynamic (MHD) bioconvection flow and heat transfer of an electrically-conducting non-Newtonian Casson thin film with uniform thickness over a horizontal elastic sheet emerging from a slit in the presence of viscous dissipation. The composite effects of variable heat, mass, nanoparticle volume fraction and gyrotactic micro-organism flux are considered as is hydrodynamic (wall) slip. The Buongiorno nanoscale model is deployed which features Brownian motion and thermophoretic effects. The model studies the manufacturing fluid dynamics of smart magnetic bio-nano-polymer coatings.

Design/Methodology/Approach – The coupled non-linear partial differential boundary-layer equations governing the flow, heat and nano-particle and micro-organism mass transfer are reduced to a set of coupled non-dimensional equations using the appropriate transformations and then solved as an nonlinear boundary value problem with the semi-numerical Liao homotopy analysis method (**HAM**).Validation with a generalized differential quadrature (**GDQ**) numerical technique is included.

Findings – An increase in velocity slip results in a significant decrement in skin friction coefficient and Sherwood number whereas it generates a substantial enhancement in Nusselt number and motile micro-organism number density. The computations reveal that the bioconvection Schmidt number decreases the micro-organism concentration and boundary-layer thickness which is attributable to a rise in viscous diffusion rate. Increasing bioconvection Péclet number substantially elevates the temperatures in the regime, thermal boundary layer thickness, nanoparticle concentration values and nano-particle species boundary layer thickness. The computations

demonstrate the excellent versatility of HAM and GDQ in solving nonlinear multi-physical nano-bioconvection flows in thermal sciences and furthermore are relevant to application in the synthesis of smart biopolymers, microbial fuel cell coatings etc.

Originality/Value – The originality of the study is to address the simultaneous effects of unsteady and variable surface fluxes on Casson nanofluid transport of gyrotactic bio-convection thin film over a stretching sheet in the presence of a transverse magnetic field. Validation of HAM with a generalized differential quadrature (GDQ) numerical technique is included.

Keywords – Magneto-hydrodynamics, Bioconvection, Nanofluid, Brownian motion, Homotopy analysis method (HAM), Generalized differential quadrature (GDQ)

Paper Type – Research paper

1. Introduction

The analysis of flow of an incompressible liquid film over a stretching sheet has important applications in many branches of science and engineering including polymer processing (extrusion), film coating and surface treatment. Thus, the understanding of flow and heat transfer within a thin film is very crucial as it features in coating processes for aerospace, chemical processing equipment, marine vessels/offshore structures and various heat exchangers. In sheet manufacturing processes, the melt issues from a slit and is subsequently stretched to achieve the desired thickness. Robust mathematical models and computational simulations of the film fluid dynamics and heat transport intrinsic to such processes provide an excellent and inexpensive mechanism for improving material design and performance. Such systems may also feature many other complex phenomena including magnetohydrodynamics (MHD), mass diffusion, Marangoni (thermo-capillary) convection, electro-hydrodynamics (EHD), thermal dispersion, non-Newtonian characteristics etc. An important contribution to simulating polymer extrusion hydromechanics was presented by Crane (1970) who studied the two-dimensional, steady boundary layer fluid flow over stretching sheet. Chakrabarti and Gupta (1979) subsequently addressed analytically the hydrodynamics and heat transfer of electrically conducting fluid flow over stretching sheet in the presence of uniform magnetic field. The exact similarity solution to the gravity driven film flow of viscous fluid is given by Andersson and Ytrehus (1985). Wang (1990) derived closed-form solutions for an unsteady stretching surface liquid film dynamics. Wang (2006) used homotopy

analysis method to study the flow and heat transfer in film flow on stretching surface. Noor et al. (2010) to analyze the magnetohydrodynamic flow and heat transfer in a thin liquid film over an unsteady elastic stretching.

The study of thin film flow of non-Newtonian fluid has received much attention as compared with its Newtonian counterpart. The transport phenomena of non-Newtonian fluids arise in many branches of chemical and materials processing engineering. The rheological properties of thin films offer interesting multi-faceted fluid dynamics problems of great relevance to technology and have therefore attracted considerable research attention. Anderson and Irgens (1988) introduced a theoretical description of laminar film flow of non-Newtonian power law fluid and have given similar solution using approximate integral method. Gorla and Nee (1989) have provided perturbation solutions for the heat transfer and heat transfer rates at ingress region of laminar power law falling liquid film flow. Pop et al. (1996) expostulated that the similarity solution obtained by Andersson and Ytrehus (1985) cannot be possible for the problems including suction/injection of fluid through porous wall. Chen (2006) investigated the convective heat transfer of non-Newtonian power-law fluids within a thin liquid film on an unsteady stretching sheet with viscous dissipation. Abel et al. (2009) examined the effect of MHD on the flow and heat transfer to a liquid film from a stretching surface.

Although several non-Newtonian models have been implemented in thin film heat transfer phenomena, relatively sparse work has been communicated on viscoplastic fluids. One example of this type of rheological fluid is the Casson fluid. According to the constitutive equation of Casson fluid model, it can reduce to viscous fluid at very high wall shear stress if yield stress is very less than the wall stress. Casson fluid model (Casson, 1959; Nakamura and Sawada,1988; Ng, 2013; Gireesha et al., 2017) is a robust viscoplastic material model which deals with the shear thinning characteristics and features a yield stress and high shear viscosity. This fluid approximates quite accurately a diverse array of biological fluent media, dense detergents, molten chocolate, cosmetics, nail polish, petroleum drilling fluids, blood, etc.

Nanofluids are synthesized by suspending nanometer-sized particles of carbides, oxides, metals, nitrides, or nanotubes in conventional fluids (water, air, oils etc.). Nanofluids have been shown both experimentally and theoretically to hold great potential in the enhancement of heat transfer properties, such as thermal diffusivity, thermal conductivity, viscosity and convective heat transfer coefficient relative to the traditional heat transfer fluids. Nanofluids have effective

applications in cleaning oil from the surface and as well as in the field of enhanced oil recovery (EOR) (Wang et al., 2013). Recently they have also been confirmed experimentally to exhibit excellent lubricity and mobility properties for petroleum drilling operations (Bég et al., 2018). Several mathematical models have already been developed to depict the thermal performance of nanofluids including the homogenous model (Choi, 1995), the dispersion model (Xuan and Roetzel, 2006) and the Buongiorno two-component model (Buongiorno, 2006). Several simulations of nanofluid dynamics pertaining to either Newtonian or non-Newtonian constitutive models in different domain with various velocity and thermal boundary conditions can be found in the scientific literature (Rashidi et al, 2014; Dinarvand et al., 2015; Kameswaran et al, 2016; Mahanthesh et al, 2016; Gorla and Vasu, 2016; Kashani et al, 2019).

Bioconvection has been observed for over a century in medical sciences (Wager, 1911; Kessler et al, 1992). The term bioconvection indicates motion of motile microorganism persuades macroscopic motion (convection). The phenomenon of bioconvection is caused by the density gradient generated by the self-propelled motile microorganisms which are a little denser than water in suspensions. The micro-organisms respond to different stimuli (taxes including light (photo-tactic), magnetic field (magneto-tactic), chemical concentration (chemo-tactic) and torque (gyro-tactic)). Recently bioconvection in nanofluids containing gyrotactic microorganisms has mobilized intensive interest due to significant potential in biomedical systems. Kuznetsov (2010) studied hydrodynamic stability in bioconvection in a horizontal layer filled with a nanofluid containing gyrotactic microorganisms and uses the micro-organisms to induce/enhance convectional process in a nanofluid. Aziz et al. (2012) demonstrated that bioconvection parameters strongly influence the heat, mass and motile microorganism transport rates in boundary layer free convection flows in a porous medium filled by a water-based nanofluid containing gyrotactic microorganisms. Beg et al. (2013) presented computational solutions for steady-state boundary layer flow of a nanofluid from an impermeable vertical flat wall in a porous medium saturated with a water-based dilute nanofluid containing oxytactic microorganisms. MHD nanofluids containing gyrotactic microorganisms near a vertical wavy surface saturated in non-Darcy medium were discussed by Ahmed and Mahdy (2016) who focused on Brownian motion and thermophoresis effects. Latiff et al. (2016) obtained Maple quadrature numerical solutions for unsteady forced convective slip boundary layer flow of a micropolar bio-nanofluid over a stretching/shrinking sheet. Raees et al. (2015) studied mixed convection in gravity-induced film flow of a fluid containing both gyrotactic

microorganisms and nanoparticles along a vertical wall with passive and the active boundary conditions. It is shown in the study that the model for passively controlled nanofluid can be easily applied and achieved in real life situations than the actively controlled model.

In light of the above extensive studies, it is evident that thus far the problem of two-dimensional laminar magnetohydrodynamic bio-convection flow of a non-Newtonian Casson nanofluid thin film with the uniform thickness over a horizontal elastic sheet in the presence of viscous dissipation has not been considered in the literature. This is the focus of the current work. To the best of authors' knowledge, no investigation have been reported addressing the simultaneous effects of unsteady and variable surface fluxes on Casson nanofluid transport of thin film over a stretching sheet in the presence of a transverse magnetic field. The coupled system of non-linear partial differential equations reduced to a set of coupled non-linear ordinary differential equations using appropriate similarity transformations. The solution in the study is based on an approximate analytical/numerical hybrid technique known as the homotopy analysis method (**HAM**) (Liao and Pop, 2004; Liao, 2009; Rashidi et al, 2012; Dinarvand et al. 2016; Ibrahim et al., 2017) which is more straightforward and simpler to apply than existing approximate analytical methods. Validation of solutions is achieved with the generalized differential quadrature (**GDQ**) method. Moreover, variations of the local skin friction, the local Nusselt number, the local wall mass flux, as well as the local wall motile micro-organism flux with rheological and nanoscale parameters are also obtained and interpreted at length. The presence of microorganisms in nanofluid improves the stability of nanofluids and prevents agglomeration of nanoparticles which is of course directly relevant to smart coating performance and also beneficial to microfluidic device wall design. Hence the geometry of the analyzed problem may help in enhancing the mass transfer in these applications. The current study is primarily of relevance to simulating the sheet manufacturing fluid dynamics of nano-bio-polymer coatings.

2. Mathematical Model

The unsteady two-dimensional hydro-magnetic bioconvection flow, heat and mass transfer of non-Newtonian Casson thin film over elastic sheet in presence of variable heat, mass and nanoparticle volume fraction flux is considered. It is assumed that the flow is laminar and is transpiring from slit which is fixed at origin. It is supposed that the swimming direction and

velocity of the microorganism is not affected by the presence of nanoparticles. Also, the suspension of nanoparticles is dilute and stable with no chemical reaction and negligible radiative heat transfer. We follow the approach of Latiff et al. (2016) and Rees et al. (2015). The film has uniform thickness $h(t)$. Plane of the sheet is placed along x-axis and y-axis is normal to it. The schematic diagram of the model is shown in Figure 1. It is assumed that the stretching of the surface starts with the velocity $U(x,t)$ and is defined as

$$U = \frac{cx}{1-\alpha t} \tag{1}$$

Constants appearing in the equation (1) are $\alpha > 0$ and $c > 0$ and dimensions of both α and c are reciprocal of time t, where c is initial stretching rate. From (1), we notice that velocity $U(x,t)$ is valid only when $t < \alpha^{-1}$ unless $\alpha = 0$. Similarly, it is supposed that the expressions for surface heat flux $q_t(x,t)$, nanoparticle volume fraction flux $q_s(x,t)$, and microorganism flux $q_n(x,t)$ at stretching surface will vary with the power of x (distance from the slit) and t (time factor) and are defined as follows:

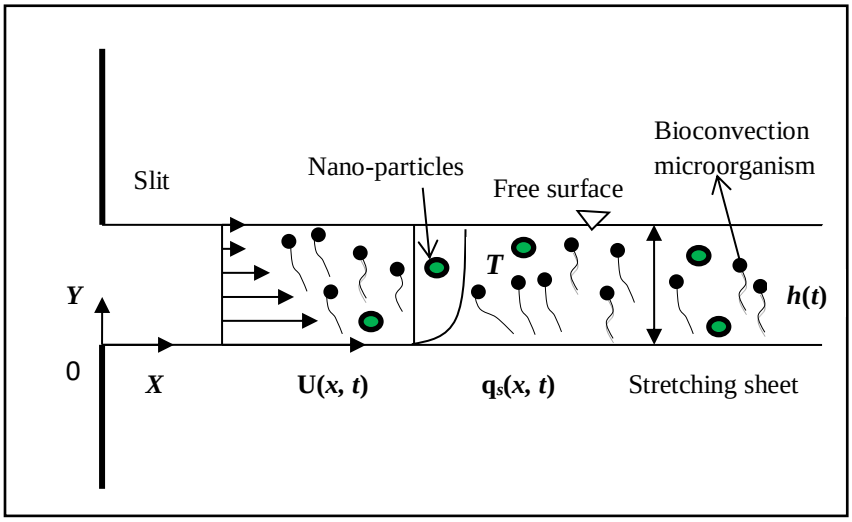

Figure 1 Schematic representation of the problem

$$q_t(x,t) = -\kappa \frac{\partial T}{\partial y} = -T_{ref} \frac{dx^{r_1}}{(1-\alpha t)^{m_1+\frac{1}{2}}} \tag{2a}$$

$$q_s(x,t) = -D_B \frac{\partial C}{\partial y} = -C_{ref} \frac{dx^{r_2}}{(1-\alpha t)^{m_2+\frac{1}{2}}} \tag{2b}$$

$$q_n(\mathrm{x},\mathrm{t}) = -D_m \frac{\partial n}{\partial y} = -n_{ref} \frac{dx^{r_3}}{(1-\alpha t)^{m_3+\frac{1}{2}}} \tag{2c}$$

κ is thermal conductivity, T_{ref}, C_{ref} and n_{ref} are reference temperature, reference concentration and reference motile density and it be taken as $0 \le T_{ref} \le T_0, 0 \le C_{ref} \le C_0$, $0 \le n_{ref} \le n_0 . m_1$, m_2 and m_3 are time indices whereas r_1, r_2 and r_3 are space indices. Further, surface temperature T_s, surface species concentration C_s and surface motile microorganism density n_s of the stretching sheet is given by

$$T_s = T_0 - T_{ref}\left(\frac{dx^{r_1}}{\kappa_1\sqrt{c/\nu}}\right)(1-\alpha\,\mathrm{t})^{-m_1} \tag{3a}$$

$$C_s = C_0 - C_{ref}\left(\frac{dx^{r_2}}{\kappa_2\sqrt{c/\nu}}\right)(1-\alpha\,\mathrm{t})^{-m_2} \tag{3b}$$

$$n_s = n_0 - n_{ref}\left(\frac{dx^{r_3}}{\kappa_3\sqrt{c/\nu}}\right)(1-\alpha\,\mathrm{t})^{-m3} \tag{3c}$$

Where T_0, C_0 and n_0 are temperature, species concentration and motile density at the slit. Here T_s, C_s and n_s are assumed to vary with distance from the slit. Constitutive equation of incompressible and isotropic non- Newtonian Casson fluid (Shateyi et al, 2017) is given by

$$\tau_{ij} = \begin{cases} 2(\mu_B + \mathrm{P}_y/\sqrt{2\phi})\,\mathrm{e}_{ij}, \phi > \varphi_c, \\ 2(\mu_B + \mathrm{P}_y/\sqrt{2\phi_c})\,\mathrm{e}_{ij}, \phi < \varphi_c. \end{cases} \tag{4}$$

Constitutive equation for Casson fluid model consists of τ_{ij}, μ_B, P_y, ϕ, e_{ij} and φ_c, where τ_{ij} is stress tensor, μ_B is plastic dynamics viscosity, P_y denotes yield stress of the fluid, ϕ is product of deformation rate with itself i.e.

$$\phi = \mathrm{e}_{ij}\mathrm{e}_{ij} \tag{5}$$

e_{ij} corresponds to the $(i, j)^{\text{th}}$ component of deformation rate. It should be noted that the fluid will behave like solid when yield stress is greater than the shear stress while it shows flow characteristics when shear stress is greater than yield shear stress.

Using these assumptions, the boundary layer equations governing the conservation of mass, linear momentum, thermal energy, nanoparticles volume fraction (species concentration) and density of motile microorganisms (Buongiorno, 2006; Kuznetsov, 2010) may be presented as follows:

Conservation of mass

$$\frac{\partial u}{\partial x}+\frac{\partial v}{\partial y}=0 \tag{6}$$

Conservation of momentum

$$\frac{\partial u}{\partial t}+u\frac{\partial u}{\partial x}+v\frac{\partial u}{\partial y}=\nu(1+\frac{1}{\beta})\frac{\partial^2 u}{\partial y^2}-\frac{\sigma^* B^2}{\rho_f}u \tag{7}$$

Conservation of thermal energy

$$\frac{\partial T}{\partial t}+u\frac{\partial T}{\partial x}+v\frac{\partial T}{\partial y}=\frac{1}{\left(\rho c_p\right)_f}\frac{\partial}{\partial y}\left(\kappa\frac{\partial T}{\partial y}\right)+\tau\left(D_B\frac{\partial C}{\partial y}.\frac{\partial T}{\partial y}+\frac{D_T}{T_\infty}\left(\frac{\partial T}{\partial y}\right)^2\right)+\frac{\mu_f}{\left(\rho c_p\right)_f}(1+\frac{1}{\beta})\left(\frac{\partial u}{\partial y}\right)^2 \tag{8}$$

Conservation of nanoparticle volume fraction (nano-species concentration)

$$\frac{\partial C}{\partial t}+u\frac{\partial C}{\partial x}+v\frac{\partial C}{\partial y}=D_B\frac{\partial^2 C}{\partial y^2}+\frac{D_T}{T_\infty}\frac{\partial^2 T}{\partial y^2} \tag{9}$$

Conservation of density of motile microorganisms

$$\frac{\partial n}{\partial t}+u\frac{\partial n}{\partial x}+v\frac{\partial n}{\partial y}+\frac{bw_c}{C_s-C_0}\left(\frac{\partial}{\partial y}\left(n\frac{\partial C}{\partial y}\right)\right)=D_m\frac{\partial^2 n}{\partial y^2} \tag{10}$$

Variables u , v , T , C and n are velocity along x-direction, velocity along y-direction, temperature of nanofluid, nano-species concentration and motile organism's density respectively. In equation (7), ν is kinematic viscosity, ρ_f represents density of fluid, B is electromagnetic strength, σ^* is Stefan- Boltzmann constant and $\beta=\mu_B\sqrt{2\phi_c}\,/\,P_y$ is the non-Newtonian Casson fluid parameter. In equation (8), κ is the thermal conductivity, D_B is the Brownian diffusion coefficient of the species and c_p is heat capacity. In equation (9), T_∞ are the ambient temperature, respectively, and C and C_∞ are the species concentration and the ambient concentration. Further, in equation (10), D_m , C_0 and C_s are motile diffusion coefficient, nanoparticle volume fraction at slit and surface species concentration respectively.

The boundary conditions for the model is

$$\begin{aligned} &u=U(\mathrm{x},\mathrm{t})+\mathrm{N}_1\left(1+\frac{1}{\beta}\right)\frac{\partial u}{\partial y}, \quad v=0, \quad -k_1\frac{\partial T}{\partial y}=q_t(\mathrm{x},\mathrm{t}),\\ &D_B\frac{\partial C}{\partial y}+\frac{D_T}{T_\infty}\frac{\partial T}{\partial y}=0, \qquad\qquad -D_m\frac{\partial n}{\partial y}=q_n(\mathrm{x},\mathrm{t}). \end{aligned} \qquad \text{at y=0} \tag{11}$$

$$\frac{\partial u}{\partial y}=0, \qquad \frac{\partial T}{\partial y}=0, \qquad \frac{\partial C}{\partial y}=0, \qquad \frac{\partial n}{\partial y}=0, \qquad v=\frac{dh}{dt} \qquad \text{at y=h (t)} \tag{12}$$

In above conditions,

$$N_1=N(1-\alpha\,\mathrm{t})^{\frac{1}{2}} \tag{13}$$

is the velocity slip factor and is varies with time and N is the initial value of N_1.

Introducing the following transformations:

$$\eta = \sqrt{\frac{c}{\upsilon(1-\alpha t)}}y, \qquad u = \frac{\partial \psi}{\partial y} = \frac{cx}{(1-\alpha t)} f'(\eta), \qquad v = -\frac{\partial \psi}{\partial x} = -\sqrt{\frac{c\nu}{(1-\alpha t)}} f(\eta) \quad (14a)$$

$$T = T_0 - T_{ref}\left(\frac{dx^{r_1}}{\kappa_1\sqrt{c/\nu}}\right)(1-\alpha t)^{-m_1}\theta(\eta), \qquad C = C_0 - C_{ref}\left(\frac{dx^{r_2}}{\kappa_2\sqrt{c/\nu}}\right)(1-\alpha t)^{-m_2}\phi(\eta)$$
$$n = n_0 - n_{ref}\left(\frac{dx^{r_3}}{\kappa_3\sqrt{c/\nu}}\right)(1-\alpha t)^{-m_3}\chi(\eta), \qquad \theta(\eta) = \frac{T-T_0}{T_s-T_0}, \qquad \phi(\eta) = \frac{C-C_0}{C_s-C_0} \quad (14b)$$

$$\chi(\eta) = \frac{n-n_0}{n_s-n_0}, \qquad k = k_\infty\left(1+\varepsilon\frac{T-T_0}{\Delta T}\right) \quad (14c)$$

where η is similarity variable, equations (14a-c) are valid only for $\alpha t \approx 1$, $f(\eta)$, $\theta(\eta)$, $\phi(\eta)$ and $\chi(\eta)$ are non-dimensional stream function, dimensionless temperature, nanoparticle volume fraction and micro-organism density function.

Using above Equations (14 a-c), the primitive boundary-layer equations (6) - (10) are readily transformed into the following system of nonlinear, coupled, ordinary differential equations and their associated boundary conditions:

$$\left(1+\frac{1}{\beta}\right)f''' + ff'' - f'^2 - S\left(\frac{\eta}{2}f'' + f'\right) - Mf' = 0 \quad (15)$$

$$\frac{1}{\Pr}\theta'' + \frac{\varepsilon}{\Pr}\left(\theta\theta'' + (\theta')^2\right) - S\left(\frac{\eta}{2}\theta' + m_1\theta\right) - r_1\theta f' + \theta' f + Nb\theta'\phi' + \mathrm{Nt}(\theta')^2 + \left(1+\frac{1}{\beta}\right)E_c(f'')^2 = 0 \quad (16)$$

$$\frac{1}{Sc}\phi'' + \frac{Nt}{Nb}.\frac{1}{Sc}\theta'' - S\left[m_2\phi + \frac{\eta}{2}\phi'\right] - r_2 f'.\phi + f.\phi' = 0 \quad (17)$$

$$\frac{1}{Sb}\chi'' - S\left[\chi.m_3 + \frac{1}{2}\chi'.\eta\right] - r_3 f'\chi + \chi' f - \frac{Pe}{Sb}\left[(\sigma+\chi)\phi'' + \chi'\phi'\right] = 0 \quad (18)$$

The boundary conditions emerge as:

$$At\ \eta = 0: \qquad f' = 1+\lambda(1+\frac{1}{\beta})f'', \quad f = 0, \quad \theta' = -1, \quad N_b\phi' + \mathrm{N}_t\theta' = 0, \quad \chi' = -1$$
$$At\ \eta = \gamma: \qquad f = \frac{S\gamma}{2}, \quad f'' = 0, \quad \theta' = 0, \quad \phi' = 0, \quad \chi' = 0 \quad (19)$$

In the reduced system of coupled nonlinear ordinary differential equations, prime represents differentiation with respect to η, dimensionless parameters arising in equations (15)-(19) are defined as: $\lambda = N\left(\frac{c}{\nu}\right)^{\frac{1}{2}}$ is the velocity (hydrodynamic wall) slip parameter, $\Pr = \frac{k_\infty}{\mu c_p}$ is the Prandtl number, $Ec = \frac{U^2}{c_p(T_s - T_0)}$ is the Eckert number. $M = \sigma B_0^2/\rho_f.c$ is the magnetic body force

parameter, $S = \alpha / c$ is unsteadiness parameter, $Nb = \tau D_B (c_s - c_0)/\nu$ is Brownian motionparameter, $Nt = \tau D_T (\mathrm{T}_s - T_0)/\nu T_\infty$ is thermophoresis parameter , $Sc = \nu / D_B$ is Schmidt number, $Sb = \nu / D_m$ is bio convection Schmidt number, $Pe = bW_c / D_m$ (bioconvection Pécletnumber), $\sigma = n_0 / (\mathrm{n}_s - \mathrm{n}_0)$ is a motile micro-organism density number ratio. Furthermore, γ represents the value of the η at the free surface. From equation (14a),free surface condition for $\eta = \gamma$ at $y = h(\mathrm{t})$, is defined as follows:

$$\gamma = \left(\frac{c}{\nu}\right)^{\frac{1}{2}} (1-\alpha t)^{-\frac{1}{2}} h(\mathrm{t}) \tag{20}$$

Value of γ can be determined by the whole data obtained in the present study. Rate of change of film thickness is given by

$$\frac{dh}{dt} = -\frac{\alpha\gamma}{2}\left(\frac{\nu}{c(1-\alpha t)}\right)^{\frac{1}{2}} \tag{21}$$

From practical application point of view, it is important to evaluate the physical quantities of flow behavior, heat and mass transfer rate by analyzing dimensionless local skin coefficient friction, local Nusselt number, local Sherwood number and motile organism number. These dimensionless parameters are defined as

$$\begin{aligned} C_{fx} &= -2\,\mathrm{Re}_x^{-\frac{1}{2}}\left(1+\frac{1}{\beta}\right) f''(0), & Nu_x &= \frac{\mathrm{Re}_x^{\frac{1}{2}}}{\theta(0)}, \\ Sh_x &= \frac{\mathrm{Re}_x^{\frac{1}{2}}}{\phi(0)}, & Nn_x &= \frac{\mathrm{Re}_x^{\frac{1}{2}}}{\chi(0)} \end{aligned} \tag{22}$$

where $\mathrm{Re}_x = \frac{Ux}{\nu}$ denotes local Reynolds number.

3. Homotopy Analysis Method

In the present study, the efficient Homotopy Analysis Method (HAM) has been implemented in order to solve the model defined by equations (15) to (18) subject to boundary conditions (19). HAM is a semi-analytical method introduced by Liao (2011) and has been deployed to solve many fluid dynamics, applied mathematics and applied mechanics problems. This method does not depend upon any physical small/large parameter and furnishes thereby a very convenient way to guarantee the series solution by using a special parameter called the convergence control

parameter. Bataineh et al. (2008) obtained series solutions to systems of first and second order partial differential equations (PDEs) by applying HAM. Rashidi and Dinarvand (2009) used HAM to study three-dimensional problem of a condensation film on an inclined rotating disk. Hayat et al. (2009) examines the boundary layer flow of carbon nanotubes over a curved stretching surface by considering Cattaneo Christov heat flux model theory. Rashidi et al. (2014) applied HAM to simulate the flow of nanofluid from a non-linearly stretching sheet with transpiration. Dinarvand et al. (2016) implemented HAM and used Tiwari-Das nanofluid model to study unsteady mixed convective stagnation-point flow of a nanofluid. Vasu and Ray (2019) applied HAM to discuss the non-similarity solution for the flow of Carreau nanofluid past vertical plate with Cattaneo-Christov heat flux model. Other applications in biological fluid dynamics and nanoscale transport include (Bég et al, 2012; Bég, et al. 2013; Tripathi and Bég, 2015; Srinivas and Bég, 2018). To extract the solutions of the (15) – (18) subjected to the boundary conditions (19) using HAM, we take the initial guesses f_0 , θ_0 , ϕ_0 and χ_0 of f , θ , ϕ and χ in the following form

$$f_0 = \left(\frac{S\gamma}{2} - \gamma \right) \frac{e^{\eta/(\lambda(1+1/\beta)} - 1}{e^{\gamma/(\lambda(1+1/\beta)} - 1} + \eta \tag{23a}$$

$$\theta_0 = -\frac{e^{\gamma-\eta}(1+\eta)}{\gamma} - \eta \tag{23b}$$

$$\phi_0 = \frac{Nt}{Nb} \left(\frac{e^{\gamma-\eta}(1+\eta)}{\gamma} + \eta \right) \tag{23c}$$

$$\chi_0 = -\frac{e^{\gamma-\eta}(1+\eta)}{\gamma} - \eta \tag{23d}$$

The linear operators are selected as follows:

$$\mathrm{L}_1(f) = f''' - f' \tag{24a}$$

$$\mathrm{L}_2(\theta) = \theta'' - \theta \tag{24b}$$

$$\mathrm{L}_3(\phi) = \phi'' - \phi \tag{24c}$$

$$\mathrm{L}_4(\chi) = \chi'' - \chi \tag{24d}$$

with the following properties:

$$\mathrm{L}_1(c_1 + c_2 e^{\eta} + c_3 e^{-\eta}) = 0 \tag{25a}$$

$$\mathrm{L}_2(c_4 e^{\eta} + c_5 e^{-\eta}) = 0 \tag{25b}$$

$$\mathrm{L}_3(c_6 e^{\eta} + c_7 e^{-\eta}) = 0 \tag{25c}$$

$$\mathrm{L}_4(c_8 e^{\eta} + c_9 e^{-\eta}) = 0 \tag{25d}$$

where c_i $(1 \le i \le 9)$are arbitrary constants. If $p \in [0,1]$ is the embedding parameter where $\hbar_1$, $\hbar_2$, $\hbar_3$ and $\hbar_4$ are the convergence control parameters, then the zeroth-order deformation equationscan be constructed as:

$$(1-p)\mathrm{L}_1[f(\eta;p)-f_0(\eta)] = p\hbar_1 \mathrm{N}_1[(f(\eta;p),\theta(\eta;p),\phi(\eta;p),\chi(\eta;p))] \tag{26a}$$

$$(1-p)\mathrm{L}_2[\theta(\eta;p)-\theta_0(\eta)] = p\hbar_2 \mathrm{N}_2[(f(\eta;p),\theta(\eta;p),\phi(\eta;p),\chi(\eta;p))] \tag{26b}$$

$$(1-p)\mathrm{L}_3[\phi(\eta;p)-\phi_0(\eta)] = p\hbar_3 \mathrm{N}_3[(f(\eta;p),\theta(\eta;p),\phi(\eta;p),\chi(\eta;p))] \tag{26c}$$

$$(1-p)\mathrm{L}_4[\chi(\eta;p)-\chi_0(\eta)] = p\hbar_4 \mathrm{N}_4[(f(\eta;p),\theta(\eta;p),\phi(\eta;p),\chi(\eta;p))] \tag{26d}$$

The appropriate forms of the boundary conditions are now:

$$f'(0,p) = 1+\lambda(1+1/\beta) f''(0,p),\ f(0,p) = 0 \text{ and } f(\gamma,p) = \frac{S\gamma}{2} \tag{27a}$$

$$\theta'(0,p) = -1,\ \theta'(\gamma,p) = 0 \tag{27b}$$

$$Nt\theta'(0,p) + Nb\phi'(0,p) = 0,\ \phi'(\gamma,p) = 0 \tag{27c}$$

$$\chi'(0,p) = -1,\ \chi'(\gamma,p) = 0 \tag{27d}$$

Based on Eqs. (15)–(18), we define the nonlinear operators as:

$$\mathrm{N}_1(f(\eta;p),\theta(\eta;p),\phi(\eta;p),\chi(\eta;p)) = \left(1+\frac{1}{\beta}\right)\frac{\partial^3 f(\eta;p)}{\partial\eta^3} + f(\eta;p)\frac{\partial^2 f(\eta;p)}{\partial\eta^2} - \left(\frac{\partial f(\eta;p)}{\partial\eta}\right)^2 - S\left(\frac{\eta}{2}\frac{\partial^2 f(\eta;p)}{\partial\eta^2} + \frac{\partial f(\eta;p)}{\partial\eta}\right) - M\frac{\partial f(\eta;p)}{\partial\eta} \tag{28a}$$

$$\mathrm{N}_2(f(\eta;p),\theta(\eta;p),\phi(\eta;p),\chi(\eta;p)) = \frac{1}{\mathrm{Pr}}\frac{\partial^2\theta(\eta;p)}{\partial\eta^2} + \frac{\varepsilon}{\mathrm{Pr}}\left(\theta(\eta;p)\frac{\partial^2\theta(\eta;p)}{\partial\eta^2} + \left(\frac{\partial\theta(\eta;p)}{\partial\eta}\right)^2\right) - S\left(\frac{\eta}{2}\frac{\partial\theta(\eta;p)}{\partial\eta} + m_1\theta(\eta;p)\right) - r_1\theta(\eta;p)\frac{\partial f(\eta;p)}{\partial\eta} + f(\eta;p)\frac{\partial\theta(\eta;p)}{\partial\eta} + Nb\frac{\partial\theta(\eta;p)}{\partial\eta}\frac{\partial\phi(\eta;p)}{\partial\eta} + Nt\left(\frac{\partial\theta(\eta;p)}{\partial\eta}\right)^2 + \left(1+\frac{1}{\beta}\right)Ec\left(\frac{\partial^2 f(\eta;p)}{\partial\eta^2}\right)^2 \tag{28b}$$

$$\mathrm{N}_3(f(\eta;p),\theta(\eta;p),\phi(\eta;p),\chi(\eta;p)) = \frac{1}{Sc}\frac{\partial^2\phi(\eta;p)}{\partial\eta^2} + \frac{Nt}{Nb}\frac{1}{Sc}\frac{\partial^2\theta(\eta;p)}{\partial\eta^2} - S\left(\frac{\eta}{2}\frac{\partial\phi(\eta;p)}{\partial\eta} + m_2\phi(\eta;p)\right) - r_2\phi(\eta;p)\frac{\partial f(\eta;p)}{\partial\eta} + f(\eta;p)\frac{\partial\phi(\eta;p)}{\partial\eta} \tag{28c}$$

$$\mathrm{N}_4\left(f(\eta;p),\theta(\eta;p),\phi(\eta;p),\chi(\eta;p)\right)=\frac{1}{Sb}\frac{\partial^2\chi(\eta;p)}{\partial\eta^2}-S\left(\frac{\eta}{2}\frac{\partial\chi(\eta;p)}{\partial\eta}+m_3\chi(\eta;p)\right)-r_3\chi(\eta;p)\frac{\partial f(\eta;p)}{\partial\eta}$$
$$+f(\eta;p)\frac{\partial\chi(\eta;p)}{\partial\eta}-\frac{Pe}{Sb}\left[(\sigma+\chi)\frac{\partial^2\phi(\eta;p)}{\partial\eta^2}+\frac{\partial\chi(\eta;p)}{\partial\eta}\frac{\partial\phi(\eta;p)}{\partial\eta}\right] \quad (28d)$$

When $p=0$ and $p=1$, we obtain

$$f(\eta;0)=f_0(\eta) \qquad f(\eta;1)=f(\eta) \quad (29a)$$
$$\theta(\eta;0)=\theta_0(\eta) \qquad \theta(\eta;1)=\theta(\eta) \quad (29b)$$
$$\phi(\eta;0)=\phi_0(\eta) \qquad \phi(\eta;1)=\phi(\eta) \quad (29c)$$
$$\chi(\eta;0)=\chi_0(\eta) \qquad \chi(\eta;1)=\chi(\eta) \quad (29d)$$

Thus, as p increases from 0 to 1 then $f(\eta;p),\theta(\eta;p),\phi(\eta;p)$ and $\chi(\eta;p)$ vary from initial approximations to the exact solutions of the original nonlinear differential equations.

Now, expanding $f(\eta;p),\theta(\eta;p),\phi(\eta;p)$ and $\chi(\eta;p)$ in Taylor series w.r.to p; we have

$$f(\eta;p)=f_0(\eta)+\sum_{m=1}^{\infty}f_m(\eta)\,p^m \quad (30a)$$

$$\theta(\eta;p)=\theta_0(\eta)+\sum_{m=1}^{\infty}\theta_m(\eta)\,p^m \quad (30b)$$

$$\phi(\eta;p)=\phi_0(\eta)+\sum_{m=1}^{\infty}\phi_m(\eta)\,p^m \quad (30c)$$

$$\chi(\eta;p)=\chi_0(\eta)+\sum_{m=1}^{\infty}\chi_m(\eta)\,p^m \quad (30d)$$

Where

$$f_m(\eta)=\frac{1}{m!}\frac{\partial^m f(\eta;p)}{\partial p^m}\Big|_{p=0} \quad (31a)$$

$$\theta_m(\eta)=\frac{1}{m!}\frac{\partial^m\theta(\eta;p)}{\partial p^m}\Big|_{p=0} \quad (31b)$$

$$\phi_m(\eta)=\frac{1}{m!}\frac{\partial^m\phi(\eta;p)}{\partial p^m}\Big|_{p=0} \quad (31c)$$

$$\chi_m(\eta)=\frac{1}{m!}\frac{\partial^m\chi(\eta;p)}{\partial p^m}\Big|_{p=0} \quad (31d)$$

If the initial guess along with auxiliary linear operators and convergence control parameters are taken in such a way that the series (30 (a)-(d)) are convergent at $p=1$ then:

$$f(\eta)=f_0(\eta)+\sum_{m=1}^{\infty}f_m(\eta) \tag{32a}$$

$$\theta(\eta)=\theta_0(\eta)+\sum_{m=1}^{\infty}\theta_m(\eta) \tag{32b}$$

$$\phi(\eta)=\phi_0(\eta)+\sum_{m=1}^{\infty}\phi_m(\eta) \tag{32c}$$

$$\chi(\eta)=\chi_0(\eta)+\sum_{m=1}^{\infty}\chi_m(\eta) \tag{32d}$$

Differentiating Eqs (26 (a)-(d))m times w.r.to p , setting $p=0$ and then dividing with m!; we have the deformation equations of mth-order as follows:

$$\mathrm{L}_1[f_m(\eta)-\chi^*{}_m f_{m-1}(\eta)]=\hbar_1 R_f^m(\eta) \tag{33a}$$

$$\mathrm{L}_2[\theta_m(\eta)-\chi^*{}_m\theta_{m-1}(\eta)]=\hbar_2 R_\theta^m(\eta) \tag{33b}$$

$$\mathrm{L}_3[\phi_m(\eta)-\chi^*{}_m\phi_{m-1}(\eta)]=\hbar_3 R_\phi^m(\eta) \tag{33c}$$

$$\mathrm{L}_4[\chi_m(\eta)-\chi^*{}_m\chi_{m-1}(\eta)]=\hbar_4 R_\chi^m(\eta) \tag{33d}$$

The associated boundary conditions are:

$$f_m'(0)-\lambda(1+1/\beta)\,f_m''(0)=0,\ f_m(0)=0 \text{ and } f_m(\gamma)=0 \tag{34a}$$

$$\theta_m'(0)=0,\ \theta_m'(\gamma)=0 \tag{34b}$$

$$Nt\theta_m'(0)+Nb\phi_m'(0)=0,\ \phi_m'(\gamma)=0 \tag{34c}$$

$$\chi_m'(0)=0,\chi_m'(\gamma)=0 \tag{34d}$$

Where

$$R_f^m(\eta)=\left(1+\frac{1}{\beta}\right)f_{m-1}'''(\eta)+\sum_{i=1}^{m-1}f_{m-1-i}(\eta)\,f_i''(\eta)-\sum_{i=1}^{m-1}f_{m-1-i}'(\eta)\,f_i'(\eta)-S\left(\frac{\eta}{2}f_{m-1}''(\eta)+f_{m-1}'(\eta)\right)-Mf_{m-1}'(\eta) \tag{35a}$$

$$R_\theta^m(\eta)=\frac{1}{\Pr}\theta''_{m-1}(\eta)+\frac{\varepsilon}{\Pr}\sum_{i=1}^{m-1}\left(\theta_{m-1-i}(\eta)\theta_i''(\eta)+\theta'_{m-1-i}(\eta)\theta_i'(\eta)\right)-S\left(\frac{\eta}{2}\theta'_{m-1}(\eta)+m_1\theta_{m-1}(\eta)\right)$$
$$-r_1\sum_{i=1}^{m-1}\theta_{m-1-i}(\eta)\,f_i'(\eta)+\sum_{i=1}^{m-1}f_{m-1-i}(\eta)\theta_i'(\eta)+Nb\sum_{i=1}^{m-1}\theta'(\eta)\phi'(\eta)+Nt\sum_{i=1}^{m-1}\theta'_{m-1-i}(\eta)\theta_i'(\eta) \quad (35b)$$
$$+\left(1+\frac{1}{\beta}\right)Ec\sum_{i=1}^{m-1}f''_{m-1-i}(\eta)\,f_i''(\eta)$$

$$R_\phi^m(\eta)=\frac{1}{Sc}\phi''_{m-1}(\eta)+\frac{Nt}{Nb}\frac{1}{Sc}\theta''_{m-1}(\eta)-S\left(\frac{\eta}{2}\phi'_{m-1}(\eta)+m_2\phi_{m-1}(\eta)\right)$$
$$-r_2\sum_{i=1}^{m-1}\phi(\eta)_{m-1-i}\,f_i'(\eta)+\sum_{i=1}^{m-1}f_{m-1-i}(\eta)\phi_i'(\eta) \quad (35c)$$

$$R_\chi^m(\eta)=\frac{1}{Sb}\chi''_{m-1}(\eta)-S\left(\frac{\eta}{2}\chi'_{m-1}(\eta)+m_3\chi_{m-1}(\eta)\right)-r_3\sum_{i=1}^{m-1}\chi_{m-1-i}(\eta)\,f_i'(\eta)$$
$$+\sum_{i=1}^{m-1}f_{m-1-i}(\eta)\chi_i'(\eta)-\frac{Pe}{Sb}\left[\sigma\phi''_{m-1}(\eta)+\sum_{i=1}^{m-1}\left(\chi_{m-1-i}\phi_i''(\eta)+\chi'_{m-1-i}(\eta)\phi_i'(\eta)\right)\right] \quad (35d)$$

where, $\chi^*_m=\begin{cases}0,\ m\le 1\\ 1,\ m>1\end{cases}$ (36)

The general solution can be written as:

$$f_m(\eta)=f^*_m(\eta)+c_1+c_2e^{\eta}+c_3e^{-\eta} \quad (37a)$$

$$\theta_m(\eta)=\theta^*_m(\eta)+c_4e^{\eta}+c_5e^{-\eta} \quad (37b)$$

$$\phi_m(\eta)=\phi^*_m(\eta)+c_6e^{\eta}+c_7e^{-\eta} \quad (37c)$$

$$\chi_m(\eta)=\chi^*_m(\eta)+c_8e^{\eta}+c_9e^{-\eta} \quad (37d)$$

$f^*_m(\eta)$, $\theta^*_m(\eta)$, $\phi^*_m(\eta)$ and $\chi^*_m(\eta)$ are special solutions of m[th] order deformation equations and the constants $c_i\ (1\le i\le 9)$ are to be determined by using boundary conditions (34 a-d).

3.1. Convergence of HAM Solutions

The higher order deformation equations (33a)-(33d) for equations (15)–(18) subject to the boundary conditions (19) can be obtained using initial guesses f_0 , θ_0, ϕ_0 and χ_0 given in (23a)-(23d) and linear operators $L_1(f)$, $L_2(\theta)$, $L_3(\phi)$ and $L_4(\chi)$ given in (24a- 24d) with the suitable values for the non-zero control parameters $\hbar_1$, $\hbar_2$, $\hbar_3$ and $\hbar_4$ that have been obtained by plotting the $\hbar$ -curves in Figure 2. From Figure 2, it is seen that the valid regions of $\hbar_1$, $\hbar_2$, $\hbar_3$ and $\hbar_4$ are

about (-0.6, -0.2) and $\hbar_1 = \hbar_2 = \hbar_3 = \hbar_4 = -0.5$ is considered for the present study.Computations are performed in symbolic software **Mathematica** with the following values of the control parameters: $\beta = 1$, $S = 1$, $M = 1.5$, $\varepsilon = 0.1$, $\Pr = 1$, $m_1 = m_2 = m_3 = 1.5$, $r_1 = r_2 = r_3 = 2$, $Nt = Nb = 0.5$, $E_c = 0.001$, $Sc = 0.6$, $Sb = 2$, $Pe = 0.1$, $\sigma = 0.1$ $\lambda = 0.2$ and $\gamma = 1$.

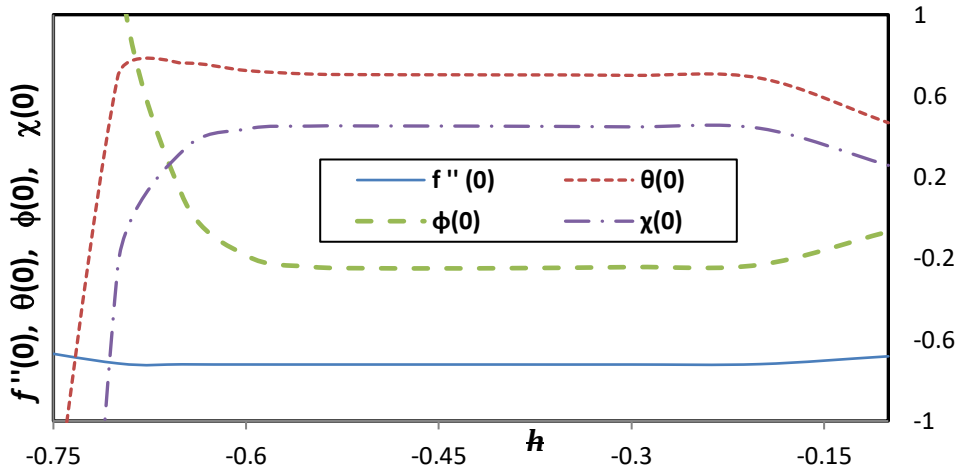

Figure 2 $\hbar$ – curve

Table I. Convergence of HAM solutions

k	$-f''(0)$	$\theta(0)$	$\varphi(0)$	$\chi(0)$
2	0.71404	0.464485	0.014451	0.206816
4	0.72181	0.654134	-0.18574	0.40339
6	0.72216	0.702721	-0.23527	0.444518
8	0.72218	0.705101	-0.24681	0.451246
10	0.72218	0.704782	-0.24819	0.452285
12	0.72218	0.706288	-0.24857	0.45257

Inspection of Table I show that the convergence of the HAM series solution (32a-32d) for different orders of approximation (k= 2, 4, 6…etc.). It is evident that the 10^{th} order (k=10) approximation is reasonable to consider for computation since further refinement does not modify the solution accuracy.

3.2. Validation with GDQ Method

The present mathematical model is a novel contribution. No existing solutions are available in the literature to validate the general HAM solutions. Therefore, we implement a different computational technique to solve the *entire general boundary value problem* as defined by (15)-(18) with respect to boundary conditions (19). The fundamental premise of generalized differential quadrature (GDQ) is that the differentiation of a function with respect to a variable of space on a given set of points is approximated as a weighted linear sum at the selected points in the domain of that variable. The GDQ approach was pioneered in fluid mechanics and engineering dynamics applications by Shu et al (1995) to improve the Bellman differential quadrature (DQM) method which is based on integral quadrature and was introduced in 1972. It generally approximates the differentiation of function with respect to space variables at a sample grid point as a weighted linear summation of all the values of function at all grid points in the domain. The basic idea for computing the weighting coefficients by GDQ is based on the analysis of a high order polynomial approximation and linear vector space. The weighting coefficients of the first order derivative are calculated by a simple algebraic formulation, and the weighting coefficients of the second and higher order derivatives are given by a recurrence relationship. Shu et al (1995) have shown that the GDQ approach is equivalent to the highest order finite difference scheme. This method is also described in some detail in the context of magnetohydrodynamics by Bég (2013). To illustrate the approximation in the GDQ, let us consider a function $f(\eta)$ defined in the domain $0 < \eta \leq a$. According to the GDQ, the function $f(\eta)$ can be approximated as follows:

$$\left.\frac{\partial^r f(\eta)}{\partial \eta^r}\right|_{\eta,\tau=\eta_i} = \sum_{m=1}^{N_\eta} A_{im}^{(r)} f(\eta_m) = \sum_{m=1}^{N_\eta} A_{ij}^{(r)} f_m , \quad i = 1, 2, \dots, N_\eta. \tag{38}$$

Therefore, the first-order derivatives have following weighting coefficients in the direction of $\eta_i$is given by the formula (Shu et al 1995; Bég, 2013).

$$A_{ij} = \begin{cases} -\sum_{j=1,\ i\neq j}^{N_\eta} A_{ij}, & i = j, \\ \frac{1}{a}\frac{M(\eta_i)}{(\eta_i - \eta_j)M(\eta_j)}, & i \neq j, \end{cases} \qquad i, j = 1, 2, \dots, N_\eta, \qquad M(\eta_i) = \prod_{j=1,\ i\neq j}^{N_\eta} (\eta_i - \eta_j) \tag{39}$$

The weighting coefficients of the higher-order derivative can be obtained as follows:

$$\left[A_{ij}^{(r)}\right] = \left[A_{ij}^{(r-1)}\right]\left[A_{ij}\right] = \left[A_{ij}\right]\left[A_{ij}^{(r-1)}\right]. \tag{40}$$

It is pertinent to deploy Chebyshev-Gauss-Lobatto grid distribution:

$$\frac{\eta_i}{a} = \frac{1}{2}\left[1 - \cos\left(\frac{i-1}{N_\eta - 1}\pi\right)\right] \qquad i = 1, 2, \ldots, N_\eta, \tag{41}$$

According to the GDQ, the discretized governing equations and the appropriate boundary conditions can then be generated, although for brevity we have omitted these lengthy algebraic expressions here. In the emerging formulations, parameters *B* and *C* arise, which represent the second- and third-order weighting coefficients, respectively. The values of the similarity flow variables i.e. f_i, θ_i , ϕ_i and $\chi_i$at each node in the solution domain can be obtained. These may then in turn be utilized to compute the wall functions i.e. skin friction, Nusselt number, Sherwood number and motile micro-organism wall mass flux. Comparisons of the HAM solutions and the GDQ code (which is executed on an SGI Octane desk workstation and takes forty seconds to converge) for skin friction coefficient, Nusselt number, Sherwood number, motile microorganisms number are presented in Table II, with all parameter data given as: $M = 1.5$, $S = 1$, $\varepsilon = 0.1$, $\lambda = 0.2$, $\mathrm{Pr} = 1$, $Sc = 0.6$, $\sigma = 0.1$, $Sb = 2$, $Pe = 0.1$, $Nt = Nb = 0.5$, $E_c = 0.001$, $\gamma = 1$ and only variation in the Casson rheological parameter, β. Excellent correlation is achieved over the entire range of β values. Confidence in the present HAM solutions is therefore justifiably very high. Furthermore Table II (and later Table III in section 4) provides a solid benchmark for other researchers to extend the current model and to compare alternative numerical methods with the present HAM and GDQ techniques.

Table II. Comparison of HAM & GDQ computations for Casson rheological parameters (β)

β	$f''(0)$ HAM	$f''(0)$ GDQ	$1/\theta(0)$ HAM	$1/\theta(0)$ GDQ	$-1/\phi(0)$ HAM	$-1/\phi(0)$ GDQ	$1/\chi(0)$ HAM	$1/\chi(0)$ GDQ
1	0.72218	0.72220	1.41888	1.41882	4.02916	4.02913	2.21099	2.21103
2	0.87756	0.87751	1.41954	1.41949	4.04312	4.04309	2.22111	2.22107
4	0.99097	0.99092	1.42176	1.42169	4.05779	4.05773	2.22982	2.22978

4. Results and Discussion

Extensive solutions derived with the HAM approach and Mathematica for the current magneto-bioconvection viscoplastic Casson thin film stretching sheet dissipative flow problem are documented in Table III and Figures 3-28.

Skin friction coefficient, Nusselt number, Sherwood number, motile micro-organisms number are displayed in Table III, respectively. Increasing values of Casson fluid parameter (β) lead to a decrease in skin coefficient friction. Skin coefficient friction, Nusselt number, Sherwood number, motile micro-organisms number are also decreasing function of Hartmann number (M) whereas they are enhanced i.e. are increasing functions of unsteadiness parameter (S). Skin coefficient friction and Sherwood number exhibit a strong decrement while Nusselt number and motile microorganism number display an increment with increasing velocity slip parameter. Rising values of Schmidt number generate a decrease in Nusselt number, Sherwood number and motile microorganism number. Bioconvection Péclet number and bioconvection constant (motile density ratio parameter) lowers the motile microorganism wall flux whereas increasing bioconvection Schmidt number raises motile microorganism number.

Table III Effect of parameters on skin coefficient friction, Nusselt number, Sherwood number and microorganism number

β	M	S	ε	λ	Pr	Sc	σ	Sb	Pe	$-f''(0)$	$1/\theta(0)$	$-1/\phi(0)$	$1/\chi(0)$
1										0.72218	1.41888	4.02916	2.21099
2										0.87756	1.41954	4.04312	2.22111
4										0.99097	1.42176	4.05779	2.22982
1	0.5									0.6734	1.42893	4.08945	2.22893
	1									0.69815	1.42385	4.05861	2.21984
	2									0.74553	1.41403	4.0011	2.20241
	1.5	0.25								1.04716	0.55474	24.9287	1.14223
		0.5								0.9341	0.89613	4.76776	1.56784
		0.75								0.82583	1.19317	4.16807	1.93705
		1	0							0.72218	1.50649	4.08292	2.21281
			0.2							0.72218	1.34726	3.95438	2.21111
			0.5							0.72218	1.16898	3.90514	2.21593
			0.1	0.1						0.95196	1.43803	4.26807	2.26692
				0.2						0.72218	1.41888	4.02916	2.21099

0.5						0.41982	1.38332	3.77378	2.13652
0.2	2					0.72218	2.20466	4.51597	2.20871
	5					0.72218	3.59776	5.50892	2.20813
	7					0.72218	0.73445	0.27511	0.47771
	1	1				0.72218	1.41379	4.2356	2.20962
		2				0.72218	1.40446	4.72947	2.20812
		5				0.72218	1.39188	5.67857	2.20798
		0.6	0			0.72218	1.41888	4.02916	2.22314
			0.2			0.72218	1.41888	4.02916	2.19898
			0.5			0.72218	1.41888	4.02916	2.16371
			0.1	1		0.72218	1.41888	4.02916	1.41787
				5		0.72218	1.41888	4.02916	3.60649
				10		0.72218	1.41888	4.02916	4.78182
				2	0	0.72218	1.41888	4.02916	2.2934
					0.2	0.72218	1.41888	4.02916	2.13107
					0.5	0.72218	1.41888	4.02916	1.90249

From Figures 3 – 6, it can be observed that as the Hartmann number $M = \sigma B_0^2 / \rho_f .c$ increases, the velocity retards slightly due to the fact that drag produced by magnetic field and the velocity close to the wall of the thin film increases gradually, which explains the emergence of the intersection in Figure 3. Meanwhile, the temperature, and motile microorganism density rise significantly whereas there is a fall in nanoparticle volume fraction as M increases (see Figures 3 – 6). Because of Lorentz force, the thermal boundary layer increase and thus magnetic field supports the temperature. Further, it is shown that the magnetic field promotes transfer of heat due to the dissipation of thermal energy since supplementary work is expended in dragging the nanofluid against the action of the magnetic field while the magnetic field emote mass transfer in a thin liquid film.

Figures 7 – 10 display the effect of unsteadiness parameter and Casson fluid parameter on the velocity, temperature, nanoparticle volume fraction and motile microorganism density. From these figures, it is observed that increasing unsteadiness parameter elevates the velocity (i.e. mobilizes flow acceleration and a thinner momentum boundary layer) and also boosts the microorganism density while suppresses the temperature and concentration. The influence of increasing Casson

fluid parameter results in elevation in the velocity and nanoparticle volume fraction profile whereas it induces a significant reduction in temperature and microorganism density number magnitudes.

Two cases are considered in Figures 11 – 15, Case I is for $r_1 = r_2 = r_3 = m_1 = m_2 = m_3 = 0$, and Case II is for $r_1 = r_2 = r_3 = 2, m_1 = m_2 = m_3 = 1.5$. The effect of Prandtl number, Casson fluid parameter, Schmidt number, bioconvection Peclet number and bioconvection Schmidt number is analysed for Case I and Case II. Here, $\hbar_1 = \hbar_2 = \hbar_3 = \hbar_4 = -0.35$ is taken for Case I and $\hbar_1 = \hbar_2 = \hbar_3 = \hbar_4 = -0.5$ is considered for Case II. Increasing bioconvection Péclet number helps in increasing the speed of the microorganisms. Fig 12 shows that the heat transfer behaviour is highly dependent on the most important parameter in thermal convection, i.e. Prandtl number $\Pr = \dfrac{k_\infty}{\mu c_p}$. The temperature of the fluid decreases monotonically with the increasing Pr in both Cases i.e. thermal boundary layer thickness is suppressed. In Figure 13, the effect of Schmidt number $Sc = \nu / D_B$ on the concentration distribution is displayed. Increasing the Schmidt number causes a decrease in the concentration profile and it is obvious that nanoparticle species diffusion is inhibited therefore with larger values of Sc and also there is an associated decrease in nanoparticle species boundary layer thickness. This behavior is due to variation in Brownian diffusion coefficient. Increasing Sc corresponds to lower Brownian diffusion coefficient which results in lesser species concentration. The same behaviour is seen in both Cases. Figure 14 shows the effect of $Pe = bW_c / D_m$ (bioconvection Péclet number) on the nanofluid characteristics. Pe features in the non-dimensional motile density conservation equation and found that it raises temperatures profile and hence elevates thermal boundary layer thickness. Likewise, rising Pe boosts the both nanoparticle concentration and the microorganism. Figure 15 demonstrates that the bioconvection Schmidt number $Sb = \nu / D_m$ helps in decreasing the microorganism concentration boundary layer thickness, and this is probably due to the fact that, viscous diffusion rate increases due to rise in Sb.

Figure 16 depicts the influence of Eckert number $Ec = \dfrac{U^2}{c_p\left(T_s - T_0\right)}$ over temperature for different Casson fluid parameter values. Rise in value of Ec leads to rise in the temperature due

to more viscous dissipation i.e. conversion of kinetic energy into thermal energy. Figure 16 also declares that the thermal boundary layer decreases with increase in Casson fluid parameter.

Figures 17 – 20 display the impact of velocity slip parameter λ on the dimensionless velocity, temperature, nanoparticle volume fraction and motile microorganism density. With the increasing values of velocity slip parameter, velocity and nanoparticle volume fraction decreases and there is an increase in temperature and microorganism density.

Figures 21 – 24 depict the influence of Brownian motion $Nb = \tau D_B (c_s - c_0)/\nu$ and thermophoresis parameter $Nt = \tau D_T (\mathrm{T}_s - T_0)/\nu T_\infty$ on the nanoparticle volume fraction and motile microorganism density. Clearly there is a marginal reduction in microorganism density with increasing Nb a similar observation is found in Kuznetsov (2012). The nanoparticle volume fraction and motile microorganism density are also influenced markedly by the thermophoresis effect. The presence of thermophoretic body force aids nanoparticle diffusion which results in enhancement of nanoparticle volume fraction. Further, increasing the Brownian motion parameter leads to lesser diameter of nanoparticles, lesser the diameter of nanoparticles corresponds to reduction in density of nanoparticle hence the nanoparticle concentration decreases.

Figures 25 – Fig 28 explore the variation of Sherwood number and motile microorganism number for thermophoresis parameter and Brownian motion parameter. Sherwood number is increased with thermophoresis effect whereas it is decreased with Brownian motion parameter. The converse trend is observed for motile microorganism number.

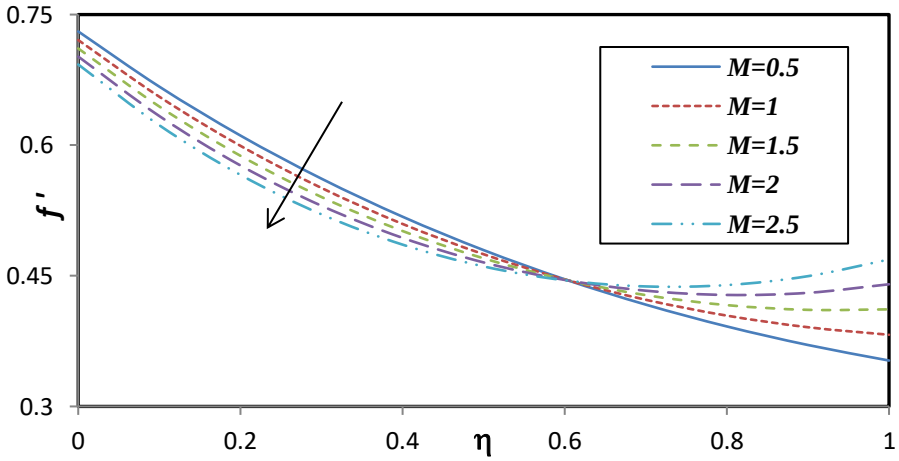

Figure 3. Effect of MHD parameter M on velocity profile

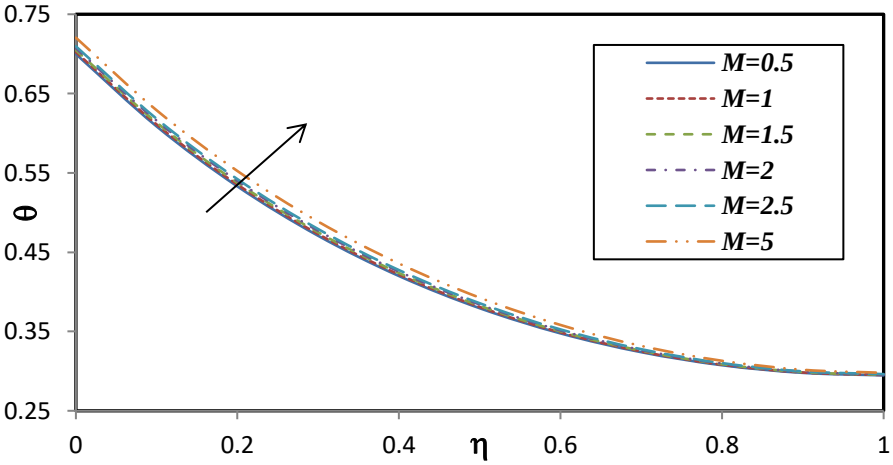

Figure 4. Effect of MHD parameter M on temperature profile

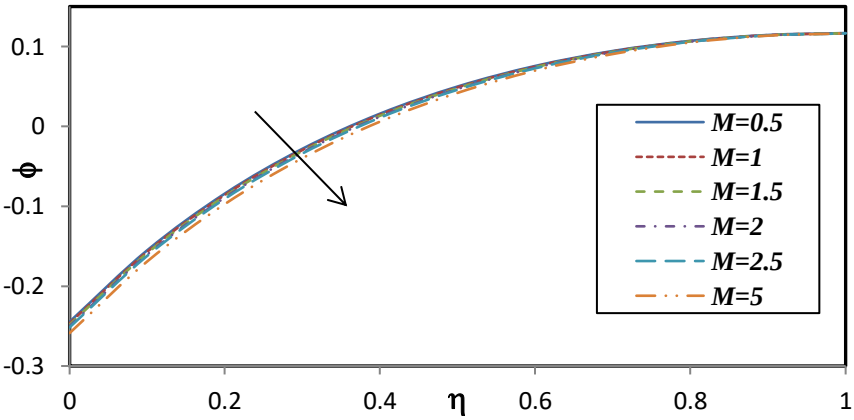

Figure 5. Effect of MHD parameter M on concentration profile

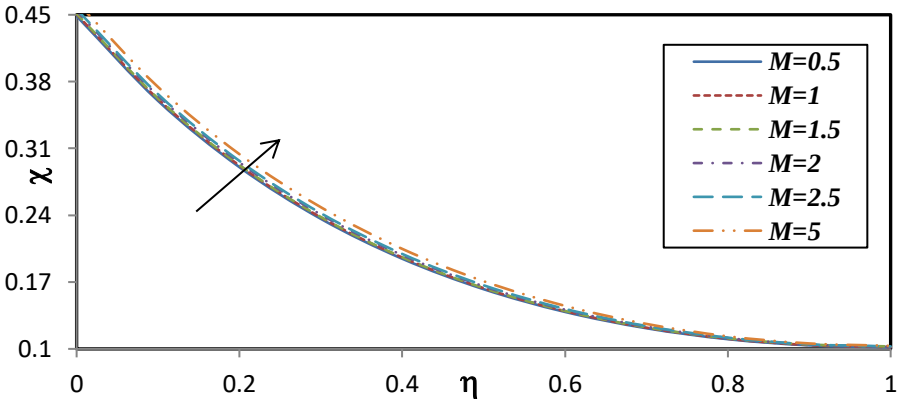

Figure 6. Effect of MHD parameter M on motile microorganism

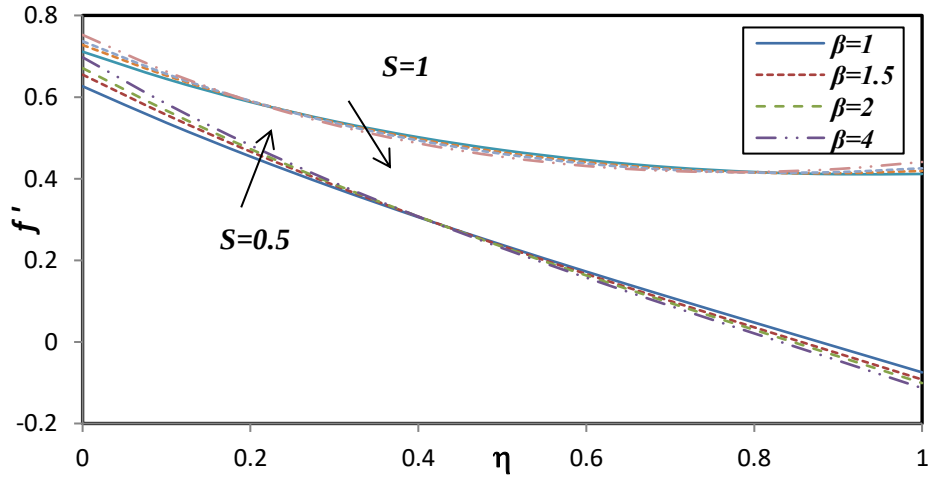

Figure 7. Impact of Casson fluid parameter β over velocity profile for different S

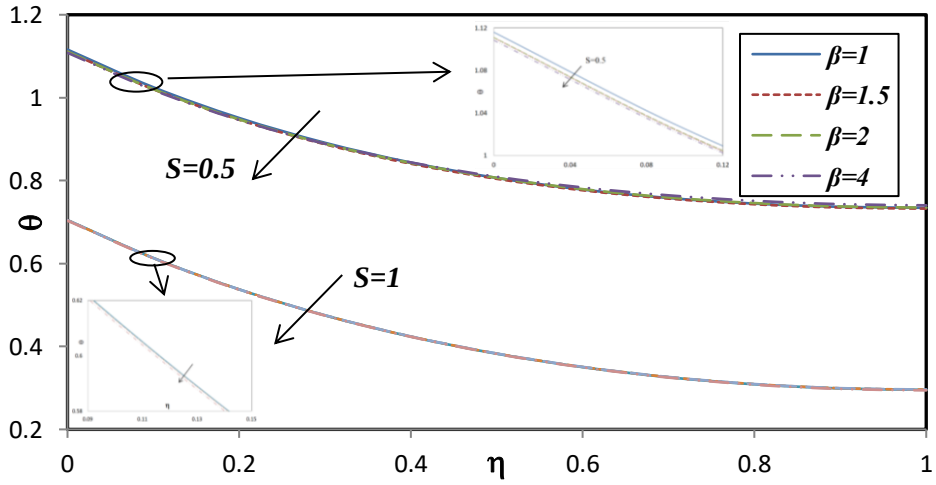

Figure 8. Impact of Casson fluid parameter β over temperature for different S

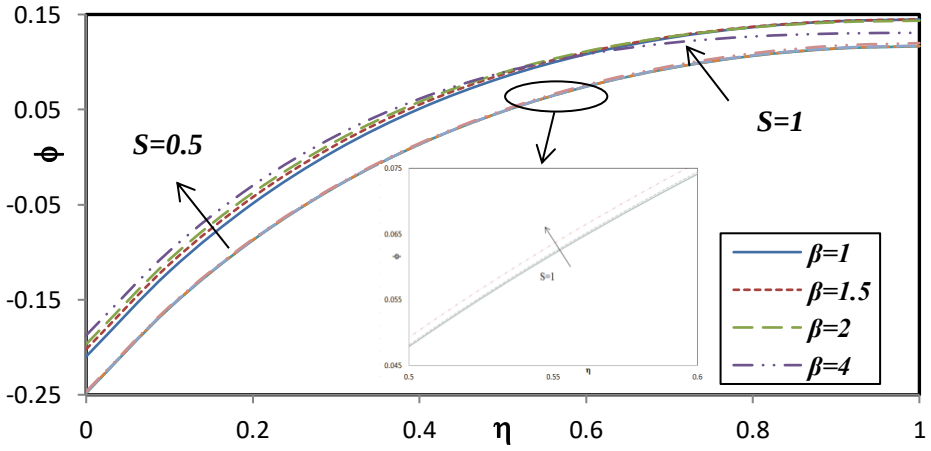

Figure 9 Impact of Casson fluid parameter β over concentration profile for different S

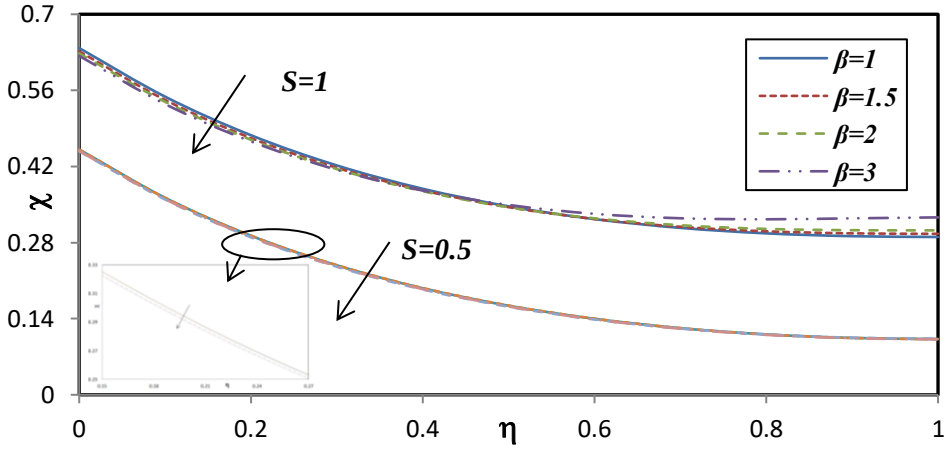

Figure 10 Impact of Casson fluid parameter β over motile micro-organism for different S

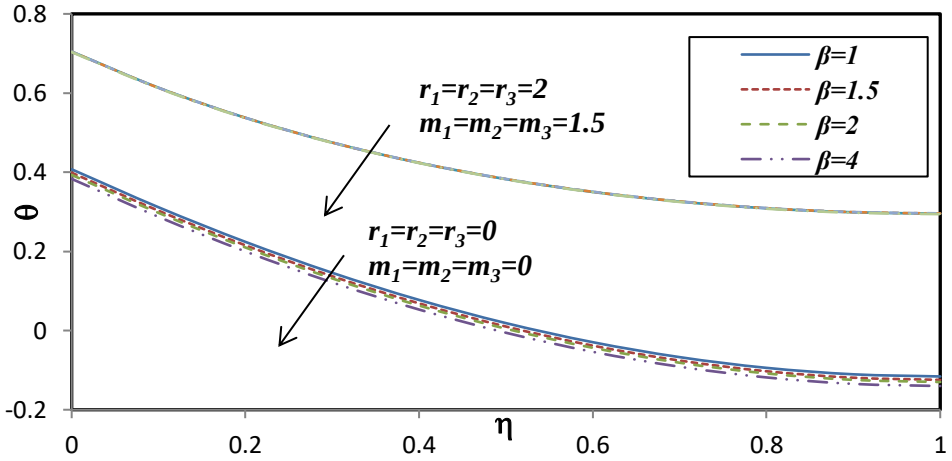

Figure 11 Effect of Casson fluid parameter β on temperature profile for Case I and Case II

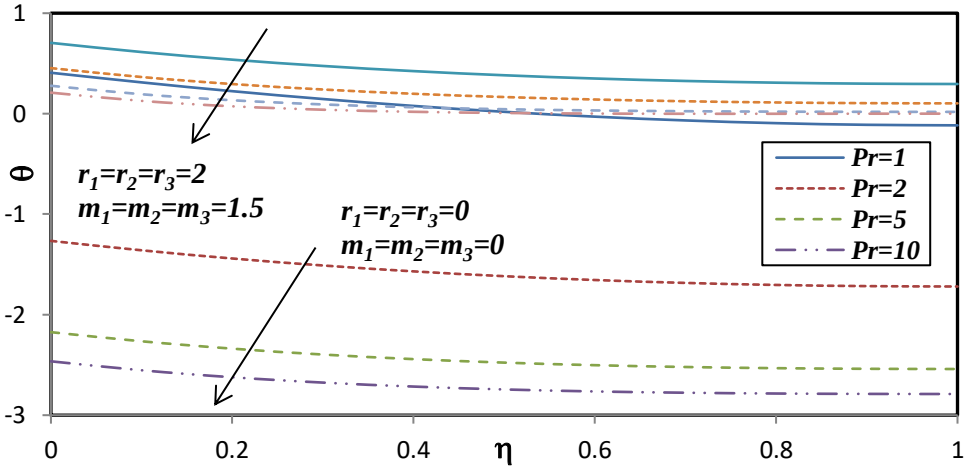

Figure 12 Effect of Prandtl number Pr on temperature for Case I and Case II

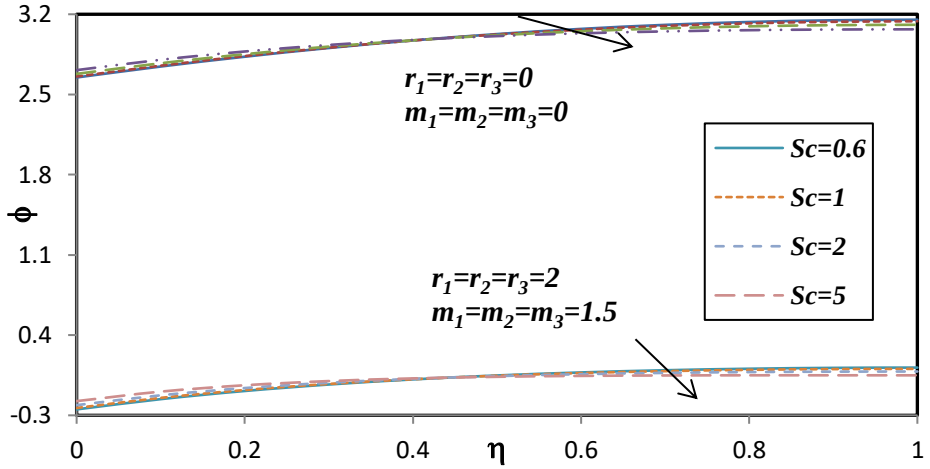

Figure 13 Impact of Sc over nanoparticle volume fraction for Case I and Case II

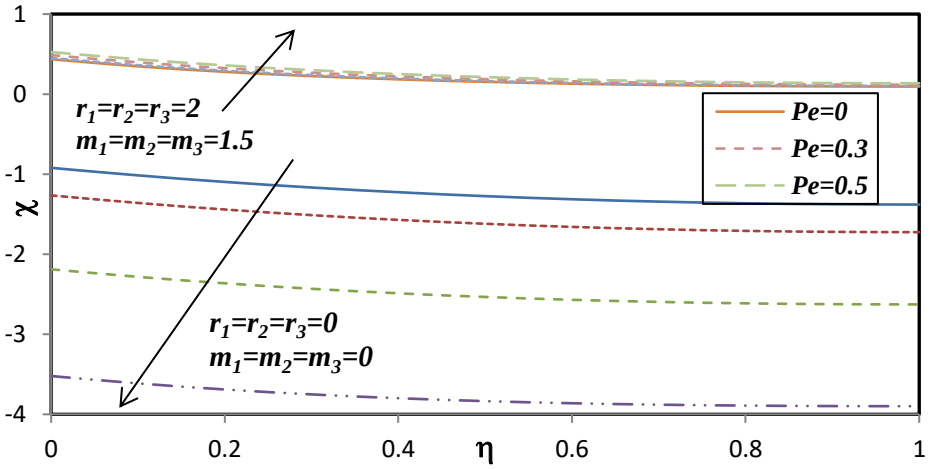

Figure 14 Impact of Peclet number Pe over motile microorganism for Case I and Case II

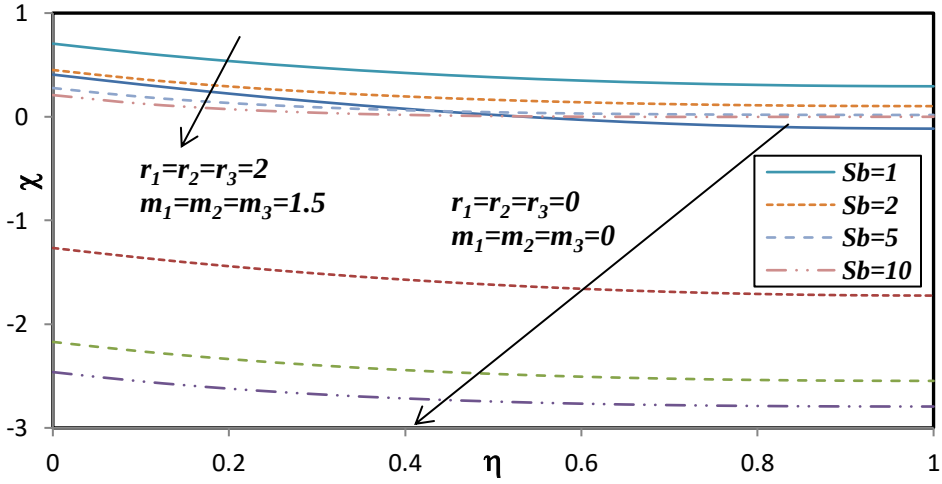

Figure 15 Impact of Sb over micro-organism for Case I and Case II

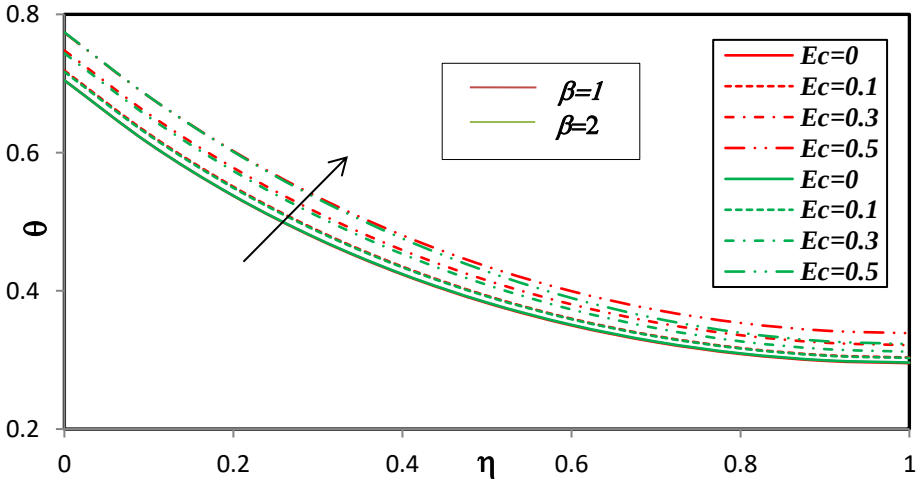

Figure 16 Impact of Ec parameter over temperature for different Casson fluid parameter

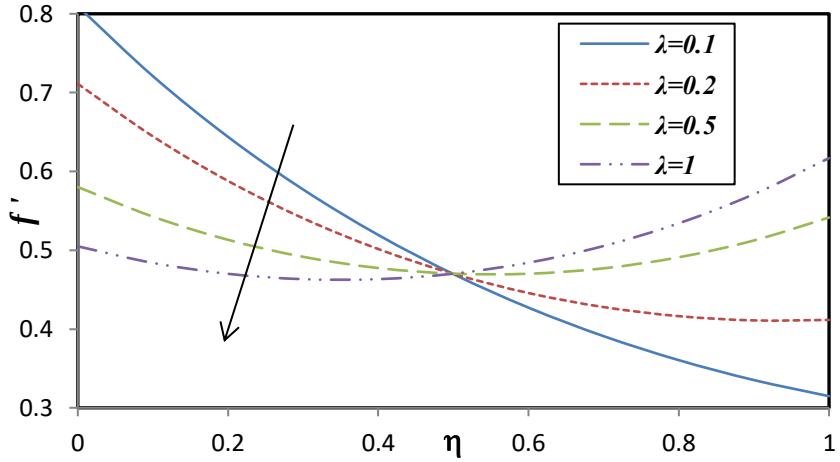

Figure 17 Impact of velocity slip parameter λ over velocity profile

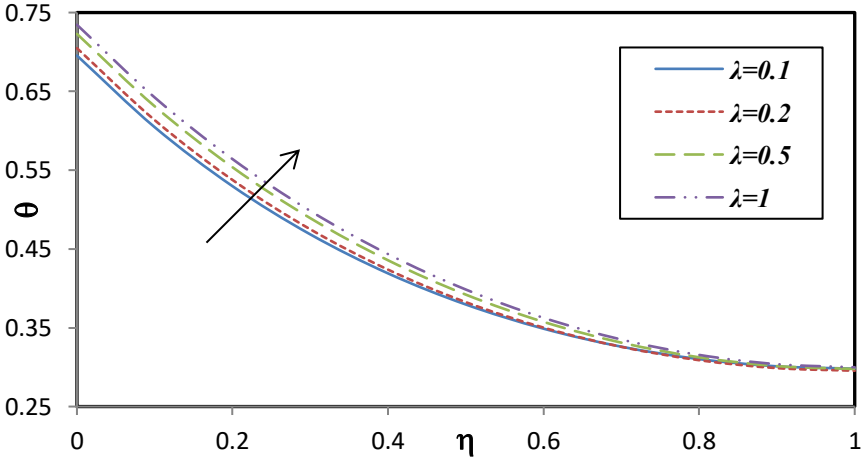

Figure 18 Impact of velocity slip parameter λ over temperature profile

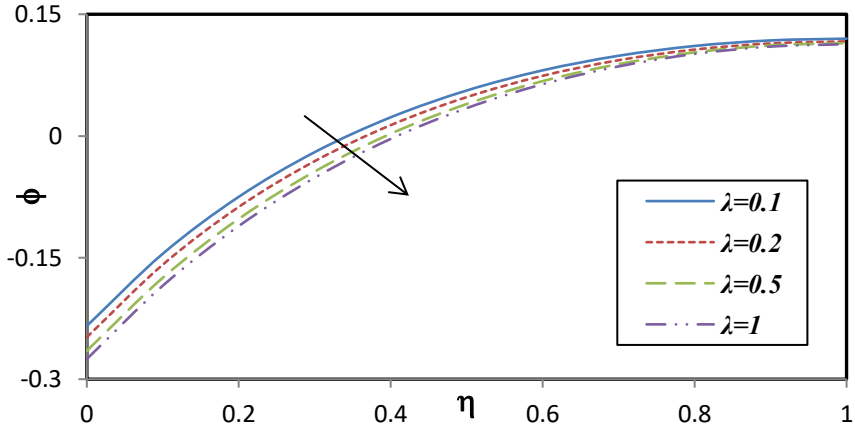

Figure 19 Impact of velocity slip parameter λ over concentration profile

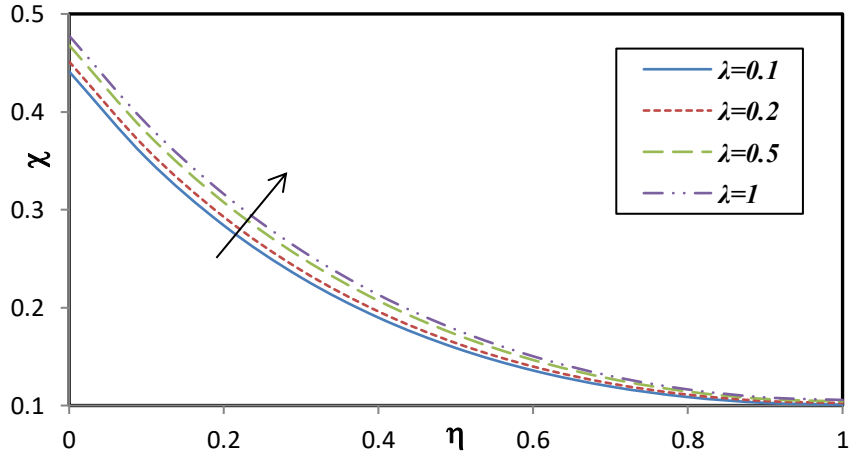

Figure 20 Impact of velocity slip parameter λ over motile microorganism

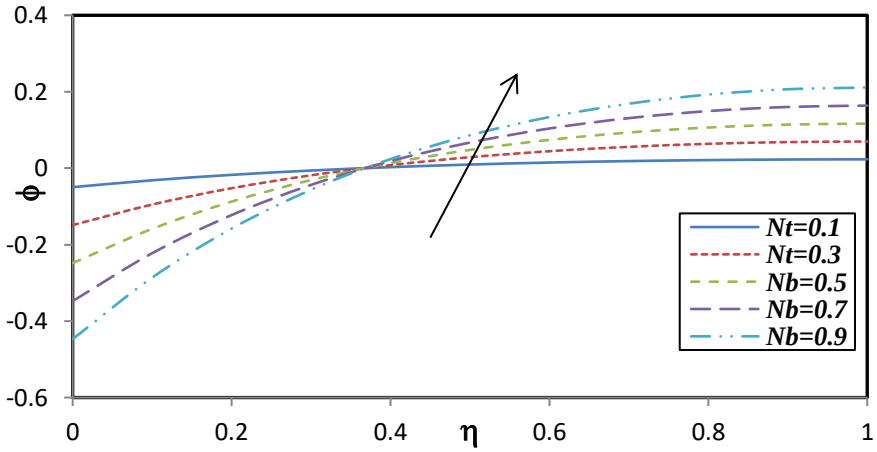

Figure 21 Impact of thermophoresis parameter over concentration profile

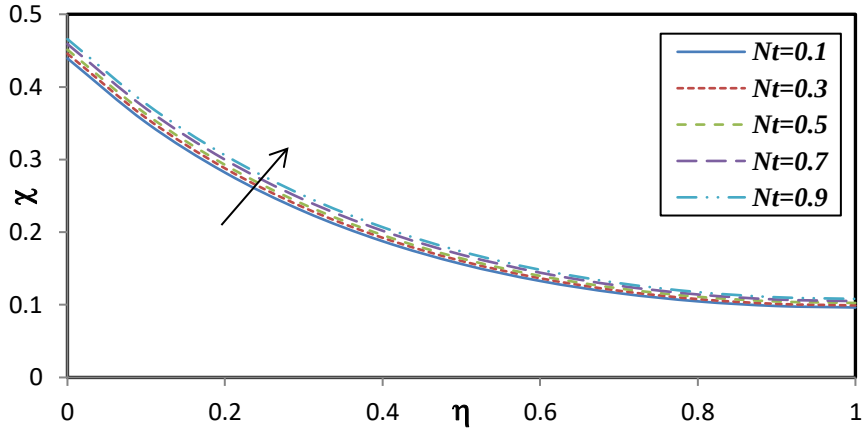

Figure 22 Impact of Brownian motion parameter over microorganism density

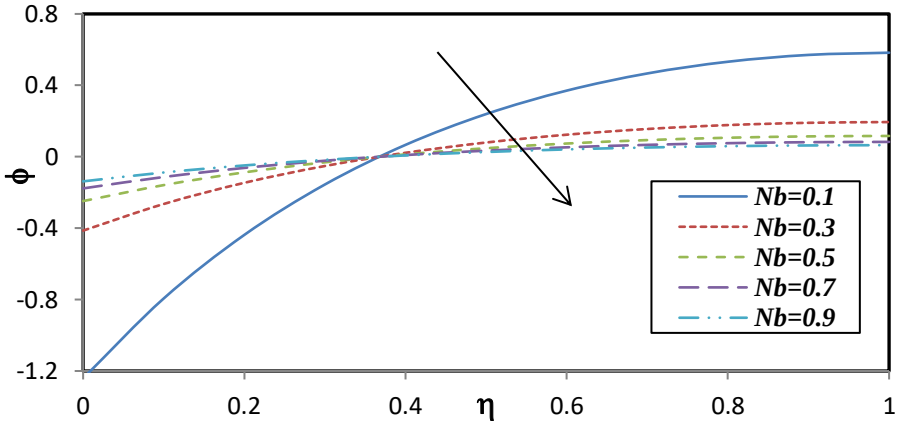

Figure 23 Impact of Brownian motion parameter over concentration profile

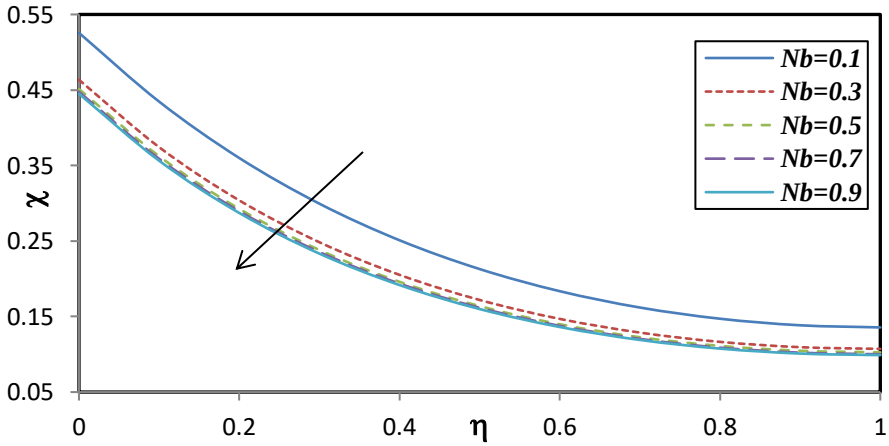

Figure 24 Impact of Brownian motion parameter over motile microorganism density

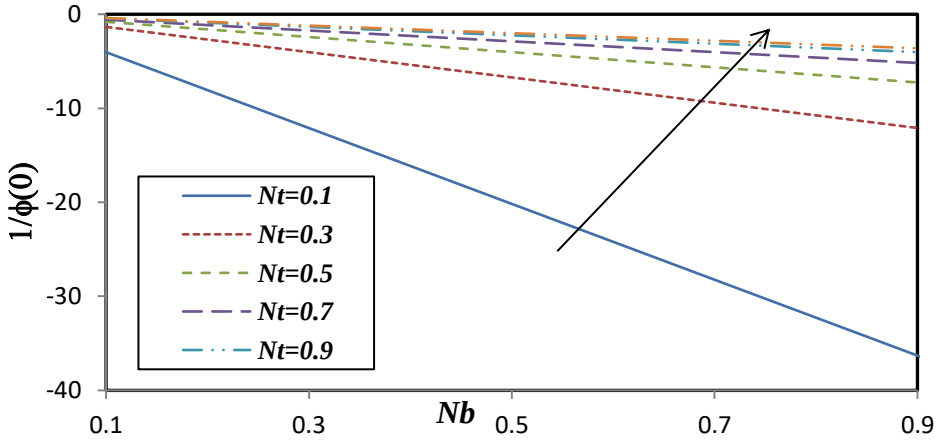

Figure 25 Variation of $1/\phi(0)$ versus Brownian motion parameter

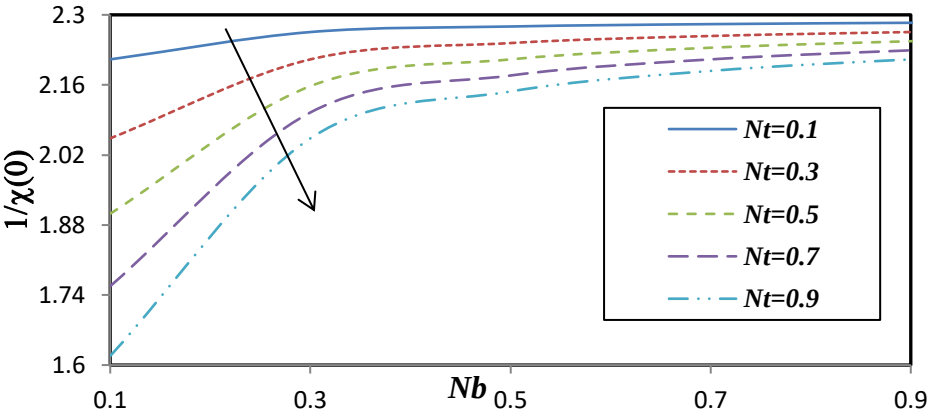

Figure 26 Variation of $1/\chi(0)$ versus Brownian motion parameter

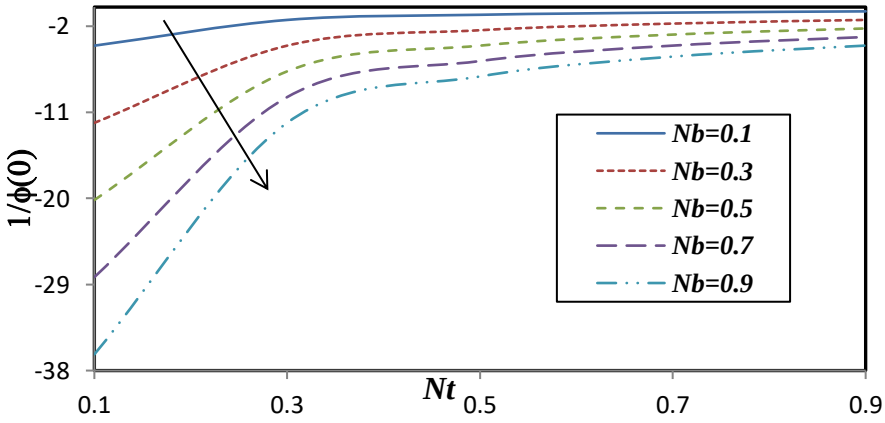

Figure 27 Variation of $1/\phi(0)$ versus thermophoresis parameter

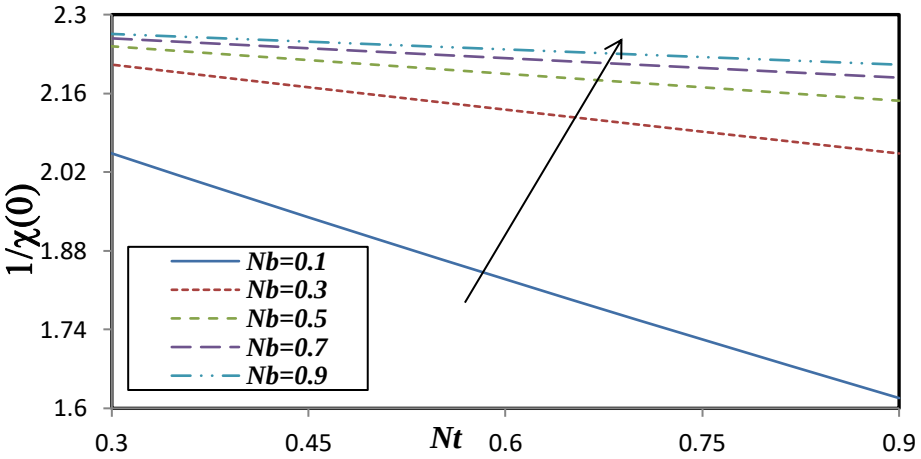

Figure 28 Variation of Sherwood Number $1/\chi(0)$ versus thermophoresis parameter

5. Conclusions

The unsteady magneto-hydrodynamic nanofluid gyrotactic bio-convection thin film boundary layer flow from a stretching sheet with viscous dissipation has been examined theoretically and numerically in this study. The normalized nonlinear partial differential boundary value problem has been transformed into an ordinary differential boundary value problem and this system has been solved with both the HAM and a generalized differential quadrature method (GDQ), demonstrating excellent agreement. A parametric study is conducted to evaluate the influence of emerging nano-scale, bio-convection and viscoplastic rheological parameters on the distributions of fluid velocity, skin friction coefficient, temperature, local Nusselt number, nano-particle volume fraction, local Sherwood number, microorganism density number function and the local density of the motile microorganism. The computations have shown that:

(i) Local skin friction coefficient, local rate of heat transfer and local density of motile microorganisms are reduced with larger values of Hartmann number (magnetic body force) whereas they are increased for larger values of unsteadiness parameter.

(ii) The velocity, temperature, and nano-particle species concentration all increase with higher values of unsteadiness parameter. Motile micro-organism flux at the wall is decreased with thermophoresis effect whereas it is increased with Brownian motion parameter.

(iii) The motile micro-organisms density number rises with velocity slip and bio-convection parameter.

(iv) Increasing Eckert (dissipation) number enhances temperatures whereas increasing Casson fluid parameter decreases them. The nanofluid temperature can be reduced by increasing Prandtl number and elevating Schmidt number causes a reduction in nano-particle species concentration.

(v) Sherwood number is increased with thermophoresis effect whereas it is decreased with Brownian motion parameter.

(vi) Increasing bioconvection Péclet number substantially elevates the temperatures in the regime, thermal boundary layer thickness, nanoparticle concentration values and nano-particle species boundary layer thickness.

(vii) Skin coefficient friction and Sherwood number exhibit a strong decrement while Nusselt number and motile microorganism number display an increment with increasing velocity slip parameter.

(viii) Greater Schmidt number depresses Nusselt number, Sherwood number and motile microorganism number.

(ix) Increasing bioconvection Péclet number and bioconvection constant (motile density ratio parameter) lowers the motile microorganism wall flux whereas increasing bioconvection Schmidt number raises motile microorganism number.

The present study has employed a simple viscoplastic model and considered magnetic field effects. Future studies will examine more complex non-Newtonian models (Tripathi et al, 2017) and also consider electrical field (electro-hydrodynamic) thin films (Gorla et al, 2004) for nanofluid bioconvection flows. The present numerical approaches (HAM and GDQ) offer excellent promise in simulating such multi-physical problems of interest in thermal thin film rheological fluid dynamics in manufacturing processes.

Acknowledgements

The authors are thankful to both reviewers for their useful and constructive comments which have helped to improve the present article.

References

Abdul Latiff, N. A., Uddin, M. J., Bég, O. Anwar and Ismail, A. I. (2016), "Unsteady forced bioconvection slip flow of a micropolar nanofluid from a stretching/shrinking sheet", IMechE Part N: J.Nanomaterials, Nanoengineering and Nanosystems, Vol. 230 No. 4, pp. 177-187.

Abel, M. S., Mahesha, N. and Tawade, J. (2009), "Heat transfer in a liquid film over an unsteady stretching surface with viscous dissipation in presence of external magnetic field", Applied Mathematical Modelling, Vol. 33 No. 8, pp. 3430-3441

Ahmed, S. E., and Mahdy, A. (2016), "Laminar MHD natural convection of nanofluid containing gyrotactic microorganisms over vertical wavy surface saturated non-Darcian porous media", Applied Mathematics and Mechanics, Vol 37 No. 4, pp. 471-484

Anderson H I. and Irgens F. (1988), "Gravity-Driven Laminar film flow of power-law fluids along vertical walls", Journal of Non-Newtonian Fluid Mechanics, Vol. 27, pp. 153-172

Andersson, H. I. and Trehus, Y T. (1985), "Falkner-Skan solution for gravity-driven film flow", ASME Journal of Applied Mechanics, Vol. 52 No. 4, pp. 783–786

Aziz, A., Khan, W. A. and Pop, I. (2012), "Free convection boundary layer flow past a horizontal flat plate embedded in porous medium filled by nanofluid containing gyrotactic microorganisms", International Journal of Thermal Sciences, Vol. 56, pp. 48-57

Bataineh, A. Sami, Noorani, M.S.M. and Hashim, I. (2008), "Approximate analytical solutions of systems of PDEs by homotopy analysis method", Computers and Mathematics with Applications, Vol. 55, pp. 2913–2923

Bég, O. A. (2013), "Numerical methods for multi-physical magnetohydrodynamics", Journal of Magnetohydrodynamics and Plasma Research, Vol. 18 no. 2, pp. 93

Bég, O. Anwar, Espinoza, D. S., Kadir, A., Shamshuddin, M. D. and Sohail, A. (2018), "Experimental study of improved rheology and lubricity of drilling fluids enhanced with nano-particles", Applied Nanoscience, pp. 1-22

Bég, O. Anwar, Rashidi, M.M., And Rahimzadeh N., Bég, T. A. and Hung, T. K. (2013), "Homotopy semi-numerical simulation of two-phase thermal haemodynamics in a high permeability blood purification device", Journal of Mechanics Medicine and Biology, Vol. 13 No. 4, pp. 1350066

Bég, O. Anwar, Prasad, V. R. and Vasu, B. (2013), "Numerical study of mixed bioconvection in porous media saturated with nanofluid containing oxytactic microorganisms", Journal of Mechanics in Medicine and Biology, Vol. 13 No. 04, pp. 1350067

Bég, T. A., Bég, O. Anwar., Rashidi, M. M. and Asadi, M. (2012), "Homotopy semi-numerical modeling of nanofluid convection flow from an isothermal spherical body in a permeable regime", International Journal of Microscale and Nanoscale Thermal and Fluid Transport Phenomena, Vol3 No. 4, pp. 67-96.

Buongiorno, J. (2006), "Convective transport in nanofluids", ASME Journal of Heat Transfer, Vol. 128 No. 3, pp. 240–250

Casson, N. (1959), Rheology of Dispersed Systems, Pergamon press, Oxford

Chakrabarti, A. and Gupta, A. S. (1979), "Hydromagnetic flow and heat transfer over a stretching sheet", Quarterly of Applied Mathematics, Vol. 37 No. 1, pp. 73-78

Chen, C. H. (2006), "Effect of viscous dissipation on heat transfer in a non-Newtonian liquid film over an unsteady stretching sheet", Journal of Non-Newtonian Fluid Mechanics, Vol. 135 No. 2, pp. 128-135,

Choi, S. U. S. (1995), "Enhancing thermal conductivity of fluids with nanoparticle", The Proceedings of the 1995 ASME International Mechanical Engineering Congress and Exposition San Francisco, pp. 99–105.

Crane, L. J. (1970), "Flow past a stretching plate, Zeitschrift für angewandte Mathematik und Physik", ZAMP, Vol. 21 No. 4, pp. 645-647

Dinarvand, S., Abbassi, A., Hosseini, R. and Pop, I. (2015), "Homotopy analysis method for mixed convective boundary layer flow of a nanofluid over a vertical circular cylinder", Thermal Science, Vol. 22 No. 2, pp. 549-561

Dinarvand, S., Hosseini, R., and Pop, I. (2016), "Homotopy analysis method for unsteady mixed convective stagnation-point flow of a nanofluid using Tiwari-Das nanofluid model" International Journal of Numerical Methods for Heat & Fluid Flow, Vol. 26 No. 1, pp. 40-62.

Dinarvand, S., Hosseini, R., Abulhasansari, M. and Pop, I. (2015), "Buongiorno's model for double-diffusive mixed convective stagnation-point flow of a nanofluid considering diffusiophoresis effect of binary base fluid", Advanced Powder Technology, 26(5), 1423-1434

Gorla, R. S. R. and Vasu, B. (2016), Unsteady convective heat transfer to a stretching surface in a non-Newtonian nanofluid, Journal of Nanofluids, Vol. 5 No. 4, 581-594.

Gorla, R., Gatica, J. E., Ghorashi, B., Ineure, P. and Byrd, L. W. (2004), "Heat transfer in a thin liquid film in the presence of an electric field", Chemical Engineering Communications", Vol. 191 No. 5, pp. 718-731.

Gorla, R. S. R. and Yong L. N. (1989), "Heat transfer in the thermal entrance region of a laminar non-Newtonian falling liquid film", International Journal of Heat and Fluid Flow, Vol. 10 No. 2, pp. 166-169

Gireesha, B. J., Archana, M., Gorla, R. S. R., Makinde, O. D. (2017), "MHD three-dimensional double diffusive flow of Casson naonofluid with buoyancy forces and nonlinear thermal radiation over stretching surface", International Journal of Numerical Methods for Heat and Fluid Flow, Vol. 27 No. 12, pp. 2858-2878.

Hayat, T., Kiran A., Imtiaz M. and Alsaed, A. (2009), "Unsteady flow of carbon nanotubes with chemical reaction andCattaneo-Christov heat flux model", Nonlinear Analysis: Real World Applications, Vol. 10, pp. 2346–2356

Ibrahim, S. M., Lorenzini, G., Kumar, P. V., Raju C. S. K. (2017), "Influence of chemical reaction and heat source on dissipative MHD mixed convection flow of a Casson nanofluid over a nonlinear permeable stretching sheet", International Journal of Heat and Mass Transfer, Vol. 111, pp. 346–355.

Kameswaran, P.K., Vasu, B., Murthy, P.V.S.N., and Gorla, R S. (2016), "Mixed Convection from a Wavy Surface Embedded in a Thermally Stratified Nanofluid saturated Porous Medium with non-Linear Boussinesq Approximation", International Communications in Heat and Mass Transfer, Vol. **77**, pp. 78-86

Kashani, D. A., Dinarvand, S., Pop, I., and Hayat, T. (2019), "Effects of dissolved solute on unsteady double-diffusive mixed convective flow of a Buongiorno's two-component non-homogeneous nanofluid", International Journal of Numerical Methods for Heat and Fluid Flow, Vol. 29 No. 1, pp. 448-466.

Kessler, J. O., Hill, N. A. and Häder, D. P. (1992), "Orientation of swimming flagellates by simultaneously acting external factors", Journal of Phycology, Vol. 28, pp. 816–822

Kuznetsov A. V. (2012), "Nanofluid bioconvection in porous media: Oxytactic microorganisms", Journal of Porous Media, Vol. 15, pp. 233-248

Kuznetsov, A. V. (2010), “The onset of nanofluid bioconvection in a suspension containing both nanoparticles and gyrotactic microorganisms”, International Communications in Heat Mass Transfer, Vol. 37 No. 10, pp. 1421-1425,

Liao, S. (2009), “Series solution of nonlinear eigenvalue problems by means of the homotopy analysis method”, Nonlinear Analysis Real World Applications, Vol. 10, pp. 2455–2470

Liao, S. (2011), Homotopy Analysis Method in Nonlinear Differential Equations, CRC Press, Florida,USA.

Liao, S.J. and Pop, I. (2004), “Explicit analytic solution for similarity boundary layer equations”, International Journal of Heat and Mass Transfer, Vol. 47, pp. 75–85

Mahanthesh, B., Gireesha, B. J., Gorla, R. R., Abbasi, F. M. and Shehzad, S. A. (2016), “Numerical solutions for magnetohydrodynamic flow of nanofluid over a bidirectional non-linear stretching surface with prescribed surface heat flux boundary”, Journal of Magnetism and Magnetic Materials, Vol. 417, pp. 189-196

Nakamura, M. and Sawada, T. (1988), “Numerical study on the flow of a non-Newtonian fluid through an axisymmetric stenosis”, ASME Journal of Biomechanical Engineering, Vol. 110, pp. 137−143

Ng, C. O. (2013), “Combined pressure-driven and electroosmotic flow of Casson fluid through a slit microchannel”, Journal of Non-Newtonian Fluid Mechanics, Vol. 198, pp. 1-9

Noor, N. F. M., Abdulaziz, O. and Hashim, I. (2010), “MHD flow and heat transfer in a thin liquid film on an unsteady stretching sheet by the homotopy analysis method”, International Journal of Numerical Methods in Fluids, Vol. 63 No.3, pp. 357-373.

Pop, I., Watanabe, T., And Konishi, H. (1996), “Gravity-driven laminar film flow along a vertical wall with surface mass transfer”, International Communications in Heat and Mass Transfer, Vol. 23, pp. 687–695

Raees, A., Xu, H., Sun, Q. and Pop, I. (2015), “Mixed convection in gravity-driven nano-liquid film containing both nanoparticles and gyrotactic microorganisms”, Applied Mathematics and Mechanics, Vol. 36 No. 2, pp. 163-178.

Rashidi, M. M., Freidoonimehr, N., Hosseini, A., Bég, O. Anwar and Hung, T. K. (2014), “Homotopy simulation of nanofluid dynamics from a non-linearly stretching isothermal permeable sheet with transpiration”, Meccanica, Vol 49 No. 2, pp. 469-482

Rashidi, M.M. and Dinarvand, S. (2009), “Purely analytic approximate solutions for steady three-

dimensional problem of condensation film on inclined rotating disk by homotopy analysis method", Nonlinear Analysis: Real World Applications, Vol. 10, pp. 2346–2356.

Rashidi, M.M., Rajvanshi, S.C. and Keimanesh, M. (2012), "Study of pulsatile flow in a porous annulus with the homotopy analysis method", International Journal of Numerical Methods for Heat and Fluid Flow, Vol. 22, pp. 971–989.

Shateyi, S., Mabood, F. and Lorenzini, G. (2017), "Casson fluid flow: Free convective heat and mass transfer over an unsteady permeable stretching surface considering viscous dissipation" Journal of Engineering Thermophysics, Vol. 26 No. 1, pp. 39-52.

Shu, C., Chew, Y. T. and Richards, B. E. (1995), "Generalized differential-integral quadrature and their application to solve boundary layer equations", International Journal for Numerical Methods in Fluids, Vol. 21, pp. 723– 733.

Srinivas, J. and Bég, O. Anwar (2018), "Homotopy study of entropy generation in magnetized micropolar flow in a vertical parallel plate channel with buoyancy effect", Heat Transfer Research, Vol. 49 No. 6, pp. 529–553.

Tripathi, D. and Bég, O. Anwar (2015), "Peristaltic pumping of Maxwell viscoelastic fluids with a slip condition: Homotopy analysis of gastric transport", Journal of Mechanics Medicine Biology, Vol. 15 No. 3, pp. 1550021.

Tripathi, D., Jhorar, R., Bég, O. Anwar and Kadir A. (2017), "Electro-magneto-hydrodynamic peristaltic pumping of couple stress biofluids through a complex wavy micro-channel", Journal of Molecular Liquids, Vol. 236, 358-367

Vasu, B., Ray, A. K. (2019), "Numerical study of Carreau nanofluid flow past vertical plate with Cattaneo-Christov heat flux model", International Journal of Numerical Methods for Heat and Fluid Flow, Vol. 29 No. 2, pp. 702–723

Wager, H. (1911), "On the effect of gravity upon the movements and aggregation of euglena viridis, Ehrb., and other micro-organisms", Proceedings of the Royal Society of London, Series B, Containing Papers of a Biological Character, Vol. 201, No. 562, pp. 303-390.

Wang, C. Y. (1990), "Liquid film on an unsteady stretching surface", Quarterly of Applied Mathematics, Vol. 48, pp. 601–10

Wang, C. (2006), "Analytic solutions for a liquid thin film on an unsteady stretching surface", Heat and Mass Transfer, Vol. 42, pp. 759–66

Wang, F. C. and Wu, H. A. (2013), "Enhanced oil droplet detachment from solid surfaces in charged nanoparticle suspensions", Soft Matter, Vol. 9, pp. 7974–7980

Xuan, Y. M. and Roetzel, W. (2006), "Conceptions for heat transfer correlation of nanofluids", International Journal of Heat and Mass Transfer., Vol. 43, pp. 3701–3707

Nomenclature

B	Strength of magnetic field
C_0	Species concentration at the Slit
c_p	Heat capacity
C_{ref}	Reference concentration
C_s	Surface species concentration of stretching sheet
C_∞	Ambient concentration
D_B	Brownian diffusion coefficient of the species
Ec	Eckert number
e_{ij}	$(i, j)^{\text{th}}$ component of deformation rate
$f(\eta)$	Non-dimensional stream function
h(t)	Thickness of the film
M	Magnetic body force parameter (Hartmann number)
m_1, m_2, m_3	Time indices
n_0	Motile micro-organism density at the slit
N_1	Velocity slip factor
N	Initial value of N_1
Nb	Brownian motion parameter
Nt	Thermophoresis parameter

n_{ref} Reference motile microorganism density

n_s Surface motile microorganism density of the stretching sheet

Nu_x Nusselt number

Pe Bioconvection Péclet number

Pr Prandtl number

P_y Yield stress of the fluid

q_t, Surface heat flux at stretching surface

q_s, Nanoparticle volume fraction flux at stretching surface

q_n Microorganism flux at stretching surface

r_1, r_2, r_3 Space indices.

Re_x Reynolds number

S Unsteadiness parameter

Sc Schmidt number

Sh_x Sherwood number

Sb Bioconvection Schmidt number

T Temperature of nanofluid

T_0 Temperature at the Slit

T_∞ Ambient temperature

T_{ref}, Reference temperature,

T_s Surface temperature of stretching sheet

u Velocity component along x directions

v Velocity component in y directions

Greek symbols

ν	Kinematic viscosity
ρ_f	Density of nanofluid
λ	Velocity (hydrodynamic wall) slips parameter
σ^*	Stefan- Boltzmann constant
β	Casson rheological parameter
κ	Thermal conductivity
σ	Motile micro-organism density number ratio
γ	Value of the η at the free surface.
τ_{ij}	Stress tensor
μ_B	Plastic dynamic viscosity in Casson model
ϕ	Product of deformation rate with itself
$\theta(\eta)$	Dimensionless temperature
$\phi(\eta)$	Dimensionless nanoparticle volume fraction
$\chi(\eta)$	Dimensionless micro-organism density function